**Contract No:**

This document was prepared in conjunction with work accomplished under Contract No. DE-AC09-08SR22470 with the U.S. Department of Energy (DOE) Office of Environmental Management (EM).

**Disclaimer:**

# *Evaluation of Hydrogen Generation in High Burnup Demonstration Dry Storage Cask*

## Spent Fuel and Waste Disposition

***Prepared for***
***US Department of Energy***
***Spent Fuel and Waste Science and Technology***

***A.L. d'Entremont***
***R.L. Kesterson***
***R.L. Sindelar***

**August 1, 2020**
**Milestone No. M3SF-20SR010207029**
**SRNL-STI-2020-00268 Revision 0**

**DISCLAIMER**

This work was prepared under an agreement with and funded by the U.S. Government. Neither the U.S. Government or its employees, nor any of its contractors, subcontractors or their employees, makes any express or implied:

1) warranty or assumes any legal liability for the accuracy, completeness, or for the use or results of such use of any information, product, or process disclosed; or
2) representation that such use or results of such use would not infringe privately owned rights; or
3) endorsement or recommendation of any specifically identified commercial product, process, or service.

Any views and opinions of authors expressed in this work do not necessarily state or reflect those of the United States Government, or its contractors, or subcontractors.

Prepared by
Savannah River National Laboratory
Aiken, South Carolina 29808

Savannah River National Laboratory®

OPERATED BY SAVANNAH RIVER NUCLEAR SOLUTIONS

# EXECUTIVE SUMMARY

This report provides a best-estimate evaluation of residual water content (post-dry out) in the High Burnup (HBU) LWR Spent Fuel Demonstration project TN-32 cask, and evaluates the radiolysis of the residual free water, and the physisorbed and chemisorbed waters on the surfaces of the fuel and cask internal contents.[1] The evaluation of radiolytic breakdown of those waters with gamma radiation causing the generation of hydrogen gas ($H_2$) is made using available literature data and models. This evaluation is part of the overall materials performance evaluation of the SNF-in-canister system, and is part of the technical bases for their continued safe dry storage.

The TN-32 cask contents included 32 HBU LWR spent fuel assemblies each with 264 fuel rods clad in zirconium alloys, aluminum neutron absorber components, and aluminum and stainless steel structural components. The residual free and surface (physisorbed/chemisorbed) waters are ascribed to water vapor in the free volume and to components' surfaces, respectively. The total potential radiolytic hydrogen inventory from the water vapor and from waters ascribed to surfaces has been calculated assuming all the water produced molecular $H_2$. The residual water that is chemically incorporated into the bulk of a hydrated oxide, i.e., chemisorbed water, and its total potential hydrogen inventory has been calculated. These calculations are at the physical limit of material available and are used for a bounding assessment purpose only.

An estimate was made of amount of hydrogen ($H_2$) generated in the HBU cask free volume after 12 days and after 40 years with radiolysis of the residual waters. The oxygen from radiolytic breakdown of free and surface water (effective net reaction H2O = H2 + 1/2O2) is not built up in the canister, and rather is assumed to be consumed by oxidation reactions with the materials. The oxidation of materials in the canister, addressed in a previous report [Shukla et al, 2019] in the NE-SFWST campaign, is not discussed in this report. No oxygen ($O_2$) generation is expected from radiolytic breakdown of chemisorbed water in hydrated oxides based on results of previous studies. Gettering of hydrogen and back reactions to reduce hydrogen concentration were not considered in this present work.

The total estimated hydrogen inventory and radiolytic hydrogen gas estimation results are shown in the table below. The assumed hydrated oxide on the aluminum, bayerite, is a tri-hydrated oxide and provides a large total source of hydrogen. The initial surface (physisorbed/chemisorbed) water ascribed to the fuel rod surfaces provides a source of rapid generation (days from dryout) of radiolytic hydrogen. For the 12-day estimate, two scenarios are considered: 1) wherein the exchange of $H_2O$ between water vapor and surface water on $ZrO_2$ and steel is neglected, and each is an isolated water reservoir (source); and 2) wherein $H_2O$ exchange between water vapor and surface water enables rapid replenishment of depleted surface water such that all free and surface water is grouped into one common reservoir. For the 40-year value, only the second scenario with $H_2O$ exchange between vapor and surface water is considered due to cooling of the fuel being assumed to facilitate more adsorption and the long time period for radiolysis.

[1] In any enclosure with materials (e.g. canister with fuel and canister internal structures), the residual water inventory includes water in the form of "free water," that would include a pool of water if the head space (free volume) is saturated with water vapor with a local surface temperature below the saturation temperature. If all material surface temperatures are above the saturation temperatures, and there is an inventory of free water in the enclosure, this water will be partitioned in equilibrium between water in the vapor phase and water that is "physisorbed/chemisorbed," that is in monolayers of a water film, including water in pores, on the surfaces of the materials. The radiolytic breakdown of free water with gamma radiation occurs readily with these waters on surfaces of a substrate vis-à-vis radiolytic breakdown of water as a vapor due to energy deposited into the substrate that is assumed to contribute to the radiolytic process. The residual water inventory also includes water in hydrated oxides that is also termed "chemisorbed" water. $H_2$ release only (i.e., no oxygen release) has been reported from radiolysis of chemisorbed water. Hydrogen yields from radiolysis of waters of material systems are determined empirically.

**Hydrogen production due to radiolysis in the HBU Demonstration Cask**

| **$H_2$ Source** | **Total $H_2$ inventory (ppmv)** | **$H_2$ production in 12 days (ppmv)** | | | | **$H_2$ production in 40 years (ppmv)** |
|---|---|---|---|---|---|---|
| | | **Assuming no $H_2O$ replenishment of surface water (Case 1)** | | **Assuming rapid $H_2O$ replenishment of surface water from water vapor (Case 2)** | | **Assuming $H_2O$ replenishment** |
| Free/surface water | 20554 | 0.01 | (steel) | 0.01 | (steel) | 20554 |
| | | 520.3 | ($ZrO_2$) | 16133 | ($ZrO_2$) | |
| | | 8.7 | (vapor) | 8.7 | (vapor) | |
| Chemisorbed water (bayerite on rails) | 86946 | 4.67 | | 4.67 | | 3711 |
| **Total $H_2$** | **107500** | **534** | | **16146** | | **24265** |
| Chemisorbed water (bayerite on cell matrix components) | 254816 | 13.7 | | 13.7 | | 10875 |

Notes: 1) The radiolytic hydrogen gas generation rates ("G-values") were taken from the literature for the estimation. A single constant dose rate (energy deposition rate) of $3 \times 10^{15}$ eV/g/s was used to calculate the 12-day values of radiolytic hydrogen generation. This dose rate is not tied to a specific internal location in the HBU cask but was previously used in a previous report (Shukla, 2019) in the NE-SFWST campaign. The 40-year values were estimated using the average dose rate of $(0.653)(3 \times 10^{15}$ eV/g/s) to account for exponential decay with the half-life of Cs-137 (30.05 y), starting from $3 \times 10^{15}$ eV/g/s.
2) The fuel rod surfaces are assumed with an attendant layer of $ZrO_2$ oxide and crud on which initial physisorbed/chemisorbed, and pore waters are estimated. 3) The aluminum surfaces are assumed with a bounding thick attendant layer of hydrated oxide.
4) Chemical back reactions, and gettering by zirconium, that would reduce the $H_2$ level in the cask are not estimated.

The predicted total amount of hydrogen gas in the HBU demo at the 12-day point varies is highly dependent on the assumption about water exchange between the vapor and the surface of the fuel. The prediction assuming no water exchange, 534 ppmv, matches the measured hydrogen from gas sampling (~500 ppmv) reported [Bryan et al, 2019a] for the HBU Demo. This value corresponds to full depletion of the initial water on the Zr components (with no replenishment) and thus is almost exclusively determined by the initial assumptions of about surface water on the Zr surface rather than being a firm verification of the inputs and methodology for estimating the radiolysis. In the other scenario with water vapor replenishing the surface water immediately, the 12-day prediction increases to >16000 ppmv, more than 30 times the measured value. The latter result is clearly not an accurate prediction of the in-cask behavior, both severely overestimating the measured amount of $H_2$ (~500 ppmv $H_2$) and underestimating the measured water vapor present at 12 days (17,400 ppmv $H_2O$) [Bryan et al, 2019a].

These results illustrate the need for testing to refine understanding of radiolysis rates, etc., in systems closely resembling the SNF-in-canister materials system. The simplified analysis here is useful for revealing which areas of the current estimate are high priorities for refinement. In this case, the predictions indicate qualitatively that the radiolysis of water on the fuel (with $ZrO_2$) overwhelmingly dominates the predicted $H_2$ generation in the short term and that this should be a primary target of experimental efforts to refine understanding of the $H_2$ generation in the cask.

It is the opinion of the authors that the estimation of the hydrogen generation rate via radiolysis in a multi-component materials/chemical system may not be reliable due to the various contributors to the radiolytic hydrogen production and the various testing methods to determine radiolytic hydrogen generation. Radiolysis test methods do not have consensus standard testing methods. Due to the system dependence of measured radiolytic yields, empirical measurement in a test system similar to the SNF-in-canister system

is recommended to benchmark a materials model of an SNF-in-canister system. This would improve understanding of radiolysis breakdown of waters and radiolytic gas generation. A laboratory-scale test involving surrogate specimens to represent the materials in the canister is suggested.

This report fulfills the M3 milestone M3SF-20SR010207029, *Radiolysis Evaluation of Bound Water in Hydrated Oxides* under Work Package Number SF-20SR01020702.

# ACKNOWLEDGEMENTS

The authors thank Sylvia Saltzstein and Charles Bryan at Sandia National Laboratories for their review comments and Charles for additional discussions on phenomenological behavior of waters; Keith Waldrop of the Electric Power Research Institute for his review comments and information on the HBU Demo project and the TN-32 cask; and John Kessler, of J Kessler and Associates, LLC, for his thorough review comments and challenging questions to help us achieve a defensible report.

# TABLE OF CONTENTS

1. INTRODUCTION ..... 1

2. POTENTIAL WATER AND HYDROGEN SOURCES IN THE HBU DEMO CASK ..... 2
2.1. HBU Demo Cask Geometry ..... 3
2.1.1. Cask Interior ..... 3
2.1.2. Cell Matrix ..... 3
2.1.3. Support Rails ..... 4
2.1.4. Fuel Rods and Additional Zr Components ..... 5
2.1.5. Helium Backfill ..... 5
2.2. Liquid Water ..... 5
2.3. Water Vapor ..... 6
2.4. Physisorbed/Chemisorbed Water on Component Surfaces ..... 6
2.4.1. Stainless Steel ..... 7
2.4.2. Fuel Assembly ..... 8
2.4.3. Aluminum Alloys ..... 10
2.5. Water Retained in Pores and Fissures ..... 10

3. PHYSISORBED/CHEMISORBED AND PORE-RETAINED WATER SOURCES ..... 12
3.1. Weakly Physisorbed Water on Component Surfaces ..... 12
3.2. Strongly Physisorbed/Chemisorbed Surface Water ..... 12
3.2.1. Aluminum Alloy Structural Components ..... 12
3.2.2. Borated Absorber Panels ..... 13
3.2.3. Fuel Oxide ..... 13
3.2.4. Fuel Rod Crud ..... 13
3.2.5. Steel Surfaces ..... 14
3.3. Pore-Retained Water ..... 14
3.3.1. Crud ..... 14
3.3.2. Fuel Rod Oxide ..... 14

4. EVALUATION OF WATER AND ASSOCIATED HYDROGEN CONTAINED IN ALL COMPONENT SOURCES ..... 15
4.1. Steel Structurals ..... 15
4.2. Aluminum Structures ..... 15
4.2.1. Aluminum Rails ..... 16
4.2.2. Aluminum Cell Matrix Plates ..... 16
4.3. Fuel Rods and Other Zr Components ..... 16
4.3.1. Surface Physisorbed/Chemisorbed Water on Fuel Rod Surface ..... 16
4.3.2. Oxide Fissures and Flaking ..... 17
4.3.3. Crud ..... 17

4.3.4. Total Water Content Associated with Zr Surfaces ..... 17
4.4. Water Vapor ..... 17

5. RADIOLYSIS OF WATER SOURCES AND HYDROGEN GENERATION ..... 18
5.1. $G_{H2}$ Values ..... 18
5.1.1. Temperature ..... 18
5.1.2. System Environment ..... 19
5.1.3. Alloy Surface and Substrate ..... 20
5.1.4. Gamma Dose and Initial Transition Effects ..... 22
5.2. Radiolysis in Water Films Versus Water Vapor ..... 24
5.3. Radiolytic Hydrogen Production ..... 24
5.3.1. Aluminum Components ..... 24
5.3.2. Fuel Rod and Other Zr Surfaces ..... 25
5.3.3. Water Vapor ..... 25
5.3.4. Steel Surfaces ..... 25

6. RESULTS AND DISCUSION ..... 27

7. REFERENCES ..... 29

This page is intentionally left blank.

# LIST OF TABLES

Table 5-1. $G_{H2}$ measured for various $Al(OH)_3$ and AlOOH powders from two studies. Values for "large" boehmite powder ranged from 0.048 to 0.13 molecules/100 eV [Kaddissy, 2016]. ..... 21

Table 5-2. Selected data points from Figure 6-6 for replotting ..... 23

Table 5-3. Primary yields (in molecules/100 eV) of products of water radiolysis under different types of radiation at room temperature [Wang, 2013] ..... 23

Table 5-4. Primary yields of water radiolysis under γ irradiation 25°C [Youssefi, 2014], as originally reported in μmol/J and converted to molecules/100 eV ..... 24

Table 6-1 Hydrogen production due to radiolysis in the HBU Demonstration Cask ..... 27

This page is intentionally left blank.

# LIST OF FIGURES

Figure 2-1. Top view of Demo cask internals [Hering, 2016]. The photo, courtesy of AREVA TN shows cask that EPRI equipped with special instruments to measure the behavior of high burnup fuel ..... 3

Figure 2-2 Diagram of 3-D COBRA-SFS model of TN-32B basket – aluminum rails in purple, stainless steel fuel compartments in blue, and structural aluminum structures in grey (Note: diagram not to scale; thicknesses greatly exaggerated for clarity) [Fort, 2019] ..... 4

Figure 2-3. Water vapor / humidity levels inside the cask [Bryan, 2019a] ..... 6

Figure 2-4. Radial distribution of system component temperatures at the axial location of Peak Cladding Temperature for initial storage conditions (as of 7/31/2017) [Fort, 2009] ..... 7

Figure 2-5. Schematic of adsorbed water on stainless steel [Dylla, 2006] ..... 8

Figure 2-6. Fuel rods with light-to-moderate crud [Knott, 2003] ..... 9

Figure 2-7. Cross-section of heavy crud [Byers, 2010] ..... 9

Figure 2-8. Comparison of eddy current measurement of total “oxide” thickness to metallurgical measurements of crud and ZrO2 thickness [Wilson, 1999] ..... 9

Figure 2-9. Surface appearance at two M5 rod locations [Montgomery, 2018] ..... 11

Figure 2-10. Surface appearance at two ZIRLO rod locations [Montgomery, 2018] ..... 11

Figure 2-11. Examples of observed crud; (a) is noted as a thin peeling crud and (b) is a heavier flaky deposit on top of a thick oxide [Montgomery, 2018] ..... 11

Figure 5-1 Schematic of the evolution of water radiolysis products [Yousefi thesis] ..... 18

Figure 5-2. Temperature Effect on $G_{H2}$ [Elliot, 2009] ..... 19

Figure 5-3 $G_{H2}$ as a function of $NO_3^-$ concentration. [Horne, 2017] ..... 20

Figure 5-4. Effect of water vapor-HCl mixtures on $G_{H2}$ [Boyd, 1973] ..... 20

Figure 5-5. Effect of $Nb^{+5}$ doping of $ZrO_2$ on the radiolytic $H_2$ production from adsorbed water [Petrik et al., 2001] ..... 21

Figure 5-6. Hydrogen yield over time for water vapor for various radiation dose rates [Wittman, 2013] ..... 22

Figure 5-7. Data points from Figure 5-6/Table 5-2 for multiple dose rates plotted as a function of dose, with a power-law fit (G in units of molecules of $H_2$ per 100 eV energy desposited) ..... 23

This page is intentionally left blank.

# ACRONYMS

| | |
|---|---|
| ASNF | Aluminum-Clad Spent Nuclear Fuel |
| BWR | Boiling Water Reactor |
| DOE | Department of Energy |
| EM | DOE, Office of Environmental Management |
| $G_{H2}$ | Number of hydrogen molecules created per unit of energy deposited in the system |
| Gy | Gray [1 Gy = 100 Rad = 1 Joule per Kg = 6.2415 x $10^{12}$ MeV per kg] |
| HBU | High Burnup |
| INL | Idaho National Laboratory |
| kGy | kiloGray |
| LWR | Light Water Reactor |
| NE | DOE, Office of Nuclear Energy |
| PNNL | Pacific Northwest National Laboratory |
| ppmv | part per million, by volume |
| PWR | Pressurized Water Reactor |
| RH | Relative Humidity |
| SEM | Scanning Electron Microscope |
| SNF | Spent Nuclear Fuel |
| SNL | Sandia National Laboratories |
| SRNL | Savannah River National Laboratory |

This page is intentionally left blank.

# 1. INTRODUCTION

Residual water (post-drying and sealing) in a spent nuclear fuel (SNF) canister can result in corrosion and radiolysis that can affect the spent nuclear fuel and canister internal structural materials [CNWRA 2013, Shukla et al, 2019, ASTM C1553-16]. Recent work [Bryan et al., 2019a] showed that inadvertent free water (~100 ml) may remain following drying even with a dryness criterion of 3 torr pressure limit following a 30-minute hold after active drying is complete.[2]

An important phenomenon is the radiolysis of the residual free water creating $H_2$ and $H_2O_2$, an oxidizing specie that is expected to quickly break down on surfaces and cause oxidation reactions with the cladding, exposed fuel, and other materials in the canister. With radiolysis of the residual free water, and consumption of oxygen, $H_2$ would be the net product in the canister free volume. The observations from the work in 2019 [Shukla et al, 2019] showed that radiolytic breakdown while the fuel was relatively hot (compared to its cooler temperatures following years of post-discharge cool-down) would result in a higher oxidation rate of any "hot" exposed fuel ($UO_2$)[3] relative to the oxidation of the cladding. In contrast, oxidation at low fuel/cladding temperatures (< ~300°C) would occur primarily with the cladding and non-fuel materials in a canister that contains exposed fuel. Thus, characterization of the rate of radiolysis is important to refine the estimation of impacts of residual water.

Hydrogen gas is a product of radiolytic breakdown of water. Bryan [Bryan et al, 2019a] observed $H_2$ at ~500 ppmv after 12 days post dry-out of the High Burnup (HBU) Demonstration Cask. A rigorous comparison of that result to an estimate of radiolytic hydrogen production had not been made.

This present work supplements the evaluation of water sources in SNF canisters [Bryan et al., 2019b], and uses the specific materials and the configuration of the HBU cask to estimate the residual water content from all sources at the time of initial sealing.

This present work estimates the hydrogen generation via radiolytic breakdown of the waters in the HBU cask. The predicted radiolytic yield is sensitive to the accuracy of both the initial water inventory estimates and to the assumed radiolysis behavior associated with different regions/surfaces in the canister. The radiolytic yield produced at a given location in the cask (e.g., a component surface) is limited by the total amount of residual water available to be broken down at that location, which is determined by the assumptions regarding the initial residual water inventories and also how the various free and surface

[2]The U.S. NRC evaluates the drying and dryness levels for dry storage packages prior to backfilling with inert gas [taken from NUREG-1536]:

> "The following examples illustrate the accepted methods for cask draining and drying in accordance with the recommendations of PNL-6365 (Knoll, 1987):
>
> • The cask should be drained of as much water as practicable and evacuated to less than or equal to 4.0E-04 MPa (4 millibar, 3.0 mm Hg or Torr). After evacuation, adequate moisture removal should be verified by maintaining a constant pressure over a period of about 30 minutes without vacuum pump operation (or the vacuum pump is running but it is isolated from the cask with its suction vented to atmosphere). The cask is then backfilled with an inert gas (e.g., helium) for applicable pressure and leak testing. Care should be taken to preserve the purity of the cover gas and, after backfilling, cover gas purity should be verified by sampling"

[3] Exposed fuel is highly unlikely as it requires a breach in fuel cladding.

water inventories interact. In general, when a dry oxide surface is exposed to humid air, first hydroxyl groups and then some number of layers of molecular water form on the surface, depending on the relative humidity, until the surface water and water vapor are in equilibrium. If either the water vapor or surface water is depleted by a mechanism such as radiolysis, then it is expected that water will adsorb/desorb to the surface to reestablish equilibrium. The assumption of whether or not this mechanism replenishes surface water during radiolysis in the cask has major impact on the radiolysis predictions.

Radiolysis and hydrogen generation is part of the present investigations regarding the consequences of inadvertent water (post-dryout) in the NE-SFWST campaign. Hydrogen content is a measure of the extent of radiolysis that has occurred in the canister, and an indirect indicator of the residual water in a canister. It is recognized that the generation of hydrogen from radiolysis in an SNF canister does not pose a flammability concern with the application of an oxygen-limit strategy to the canister [Sindelar, et al, 2020].

# 2. POTENTIAL WATER AND HYDROGEN SOURCES IN THE HBU DEMO CASK

This discussion focuses on the water sources present in the High Burnup Demo storage cask from North Anna [Bryan et al, 2019a]. Figure 2-1 is a top view of the cask prior to loading. After the fuel assembly loading into the demo cask and in preparation for long term storage, water was drained from the cask and numerous blowdowns were done to further enhance the water removal. The drying process involved a sequence of vacuum and hold conditions with the cask (internals) subsequently brought to an initial 55 Pa (0.41 Torr) vacuum with pressure being allowed to rise for about eight hours, followed by a backfill with helium to a pressure of 32 psi ($2.2\times10^5$ Pa) [Bryan et al, 2019a]. The cask contains 32 spent fuel assemblies.

The loading of SNF into dry storage casks and the subsequent drying operation can leave small amounts of residual water in the sealed casks. This water could be in the form of:

a) Liquid water at the cask bottom or in isolated areas in the fuel assembly and cask internal structures. (This would be inadvertent free water that could only be from trapped water or frozen water at a local cold spot.)

b) Water vapor as humidity in the cask internal environment. (At a 3 torr pressure, approximately 0.43 moles of free water in the form of water vapor is assumed to remain in the canister [Knoll, 1987].)

c) Physisorbed /Chemisorbed water on component surfaces. (A partition of the free water between water vapor and monolayers of water on the surfaces will be formed.)

d) Chemisorbed water in hydrated oxides and crud films. (This refers to water that is chemically bound as hydrated oxides.)

e) Water retained strongly by capillary forces in pores and fissures in the crud and fuel rod oxide. This water is termed “physisorbed/chemisorbed” in this report. This water is expected to break down radiolytically the same as physisorbed water. (Oxides formed on the aluminum structural surfaces are relatively thin and capillary retention is assumed to be negligible.)

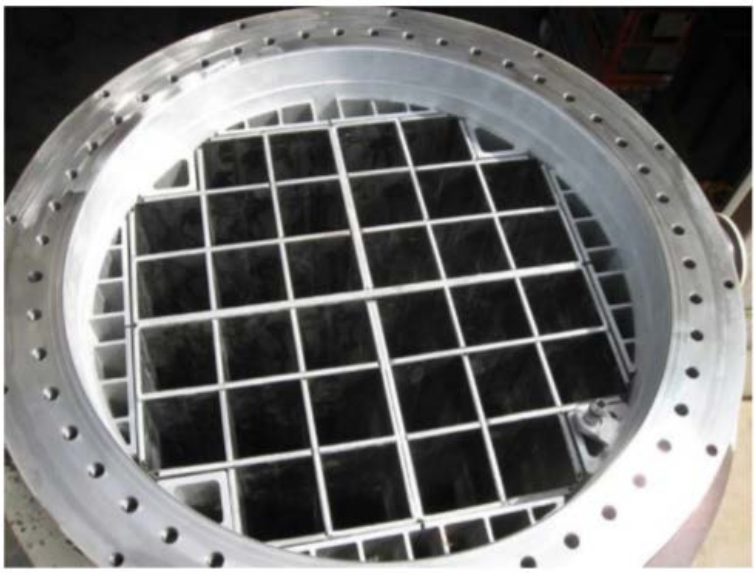

**Figure 2-1. Top view of Demo cask internals [Hering, 2016]. The photo, courtesy of AREVA TN shows cask that EPRI equipped with special instruments to measure the behavior of high burnup fuel**

## 2.1. HBU Demo Cask Geometry

Where detailed component data was not found, estimates are made regarding dimensions.

### 2.1.1. Cask Interior

The HBU Demo cask has inner dimensions of 163.250" (4.14655 m) tall and 68.750" (1.7463 m) diameter [Jenson, Drawing of TN-32 cask from Waldrop, 2020], yielding a total cask volume of 9.9309 $m^3$. The nominal free volume in the cask is estimated to be about 5.96 $m^3$ assuming a 60% internal free volume.

The same internal dimensions yield a nominal surface area for the uncoated steel liner of 27.538 $m^2$ (22.748 $m^2$ for the sides plus 4.7900 $m^2$ for the ends). Assuming only one side of the liner is exposed to the interior environment, 27.538 $m^2$ is the total surface area associated with the cask interior. The cask description includes an aluminum spray on the liner for corrosion resistance. It is not clear if the spray is on the outer diameter or the inner diameter. For this evaluation, it is assumed that the aluminum is on the outer surface and not exposed to the cask inner environment. If it is on the inner surface, it will contribute to the $H_2$ source, but not significantly over the short term.

### 2.1.2. Cell Matrix

Figure 2-2 is a schematic of the cell matrix structure used for thermal modeling and shows the structural material layout in cross-section (not to scale). The cell matrix has 32 cells to hold fuel assemblies, each 8.700 in (22.098 cm) square from wall to wall [Jenson, Drawing of TN-32 cask from Waldrop, 2020]. The walls between cells are constructed of layered plates. Per Fort [Fort et al, 2019], "the basket cells are formed […] with stainless-steel sheets on the outer faces of the basket structure. Much thicker aluminum alloy plates are sandwiched between the stainless-steel plates, with double-thickness aluminum plates forming the central 'cross' of the basket." According to the schematic for thermal modeling [Jenson, Drawing of TN-32 cask], the center "cross" cell walls are 1.080" thick (including both aluminum and steel), and the narrower cell walls are 0.540"-thick aluminum sandwiched between 0.105"-thick stainless-steel plates.

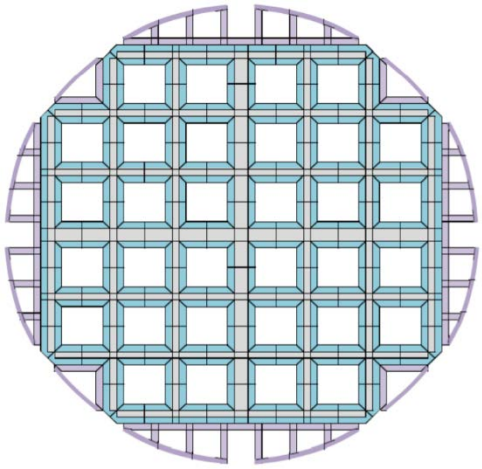

**Figure 2-2 Diagram of 3-D COBRA-SFS model of TN-32B basket – aluminum rails in purple, stainless steel fuel compartments in blue, and structural aluminum structures in grey (Note: diagram not to scale; thicknesses greatly exaggerated for clarity) [Fort, 2019]**

The interior surface area of a single cell is given by $4(8.700\text{ in})(160.000\text{ in}) = 5568\text{ in}^2 = 3.592\text{ m}^2$. The total cell surface area for all 32 cells is 115.0 $m^2$. (This is the exposed area associated with the stainless-steel cell liners.)

The total surface area of the structural aluminum plates within the cell matrix is approximately 196000 $in^2$ (126 $m^2$), and the same for the borated aluminum neutron absorber panels within the same structure [Waldrop, 2020].

### 2.1.3. Support Rails

The supporting rails positioned between the straight sides of the basket cell matrix and the curved cylinder are also aluminum and comprise a significant surface area of exposed aluminum. The surface area of the rails is more complicated to calculate than that of the basket cells, but as a first approximation, the rail plates are made up of:

- Outer curved plates roughly forming a cylinder with outer diameter 67.750” and a height of 160.000” [Jenson, Drawing of TN-32 cask]. Assuming these plates are exposed on both sides, due to clearance of the basket in the cask, this yields an area of approximately $2\pi(67.750\text{ in})(160.000\text{ in}) = 68110\text{ in}^2 = 43.94\text{ m}^2$.
- Straight plates along the outer edges of the basket cell matrix, equivalent to four plates, each the width of six basket cells and 160.000” long. The interior of each basket cell is 8.700” square; the center “cross” cell walls are 1.080” thick, and the narrower cell walls are 0.540” of aluminum sandwiched between 0.105” stainless-steel plates [Jenson, Drawing of TN-32 cask]. The width of 6 cells spans six 8.7”-wide cell interiors, one 1.080”-thick center wall, four 0.750”-thick interior walls (two stainless steel plates apiece), and two 0.645”-thick outer walls (only one stainless-steel plate), i.e., $[6(8.7\text{ in}) + 1.080\text{ in} + 4(0.750\text{ in}) + 2(0.645\text{ in})] = 57.57\text{ in}$. Therefore, the approximate area of aluminum along the four sides of the basket matrix, assuming they are exposed on one face (with the other face against the cell matrix), is $4[57.57\text{ in}](160.000\text{ in}) = 36845\text{ in}^2 = 23.77\text{ m}^2$.
- Struts connecting the outer cylindrical plates to the straight plates, six on each of the four sides of the basket. The maximum possible width of these struts can be determined by the difference between the inner radius of the curved plates (33.750” [Jenson, Drawing of TN-32 cask]) and half the width of the basket cell matrix (57.57”/2 = 28.79”) plus the 0.5”-thick straight aluminum plate [Jenson, Drawing of TN-32 cask], i.e., ≈4.5”. These supporting struts are exposed on both faces.

Roughly approximating the four centermost struts as 4.5" wide and the outermost two as half that width due to the curvature of the outer plate, the area for all four sets is approximated as $4(2)(5)(4.5\text{ in})(160.000\text{ in}) = 28800\text{ in}^2 = 18.58\text{ m}^2$.

This yields a total estimated exposed surface area of the aluminum rails of $43.94\text{ m}^2 + 23.77\text{ m}^2 + 18.58\text{ m}^2 = 86.29\text{ m}^2$. If the $253\text{ m}^2$ of aluminum area in the cell matrix ($126\text{ m}^2$ each for structural aluminum and borated aluminum panels, as described above) is included, this yields a total of about $339\text{ m}^2$ aluminum surface area. The aluminum rails and the aluminum cell matrix components are treated separately in the calculations.

### 2.1.4. Fuel Rods and Additional Zr Components

Bryan [Bryan et al, 2019b] gives the surface area of a single PWR fuel rod as $0.115769\text{ m}^2$. Each assembly contains 264 fuel rods [Bryan et al, 2019b], and the HBU Demo cask contains 32 such assemblies. This yields a total fuel rod surface area of $978\text{ m}^2$ for all rods in the cask.

Additional zirconium alloy components also exist in the fuel assemblies [Bryan et al, 2019b]. The additional area of these components is approximated here as about 37% of the fuel rod surface area.

### 2.1.5. Helium Backfill

The cask pressure is 2.2 bar, and the free volume is $5.96\text{ m}^3$. Using an estimated average temperature of 135°C and the ideal gas law, this yields an estimated 386 mol He in the cask backfill.

## 2.2. Liquid Water

Nearly complete removal of the free water from the cask was successful, as observed from gas samples taken 12 days after the backfill. Bryan [Bryan et al. 2019a] reports that, assuming a homogeneous gas phase in the cask, the humidity levels in the gas samples indicate no free liquid water, only water vapor, remaining in the cask unless liquid water had been trapped in occluded locations. At assembly loading in the pool, there is a probability that some of the thimble tubes could contain water but only if the drain hole being plugged by debris settling during storage. As discussed by Bryan [Bryan et al, 2019a,b], it is expected that the cask high-temperature drying will evaporate any water retained at loading. Thus, a thimble tube water source is not included in this evaluation.

There is a potential for boric acid $H_3BO_3$ precipitation from PWR spent fuel pool to be in the canister as discussed by Bryan et al [Bryan et al, 2019b]. At a nominal SFP concentration of 2000 ppm of boric acid, there would be 0.2 moles of boric acid per liter of pool water that evaporates in a canister. At a temperature of 150°C, full dehydration of 0.2 moles of $H_3BO_3$ would produce 0.3 moles (6 grams) of water together with boron oxide, $B_2O_3$. Due to high uncertainties of the amount of residual water following blowdown that would remain in the canister, and the amount, if any of $H_3BO_3$ that did not thermally decompose during the drying process, this potential water source is not included in this evaluation.

Thicker oxides (typically >50 microns), if present on the fuel rods, will have some degree of fissuring or incipient delamination due to the stresses generated in the oxide during formation. These fissures will act as pores to retain some water from operation and storage in the fuel pool. Upon drying for cask storage, it is postulated that the majority, if not all, of this water source will be converted to steam during the drying process and removed.

Liquid water evaluation is excluded from this study. Free water is considered to be in vapor form.

## 2.3. Water Vapor

Bryan [Bryan et al, 2019a] reported the presence of water vapor in the sampled cask gas at a level of 17,400 ppmv at 65°C. With uncertainties, a 2% (20000 ppmv) value for initial water vapor in the cask internal gas is included in the current analysis. It is reported, Figure 2-3, that the minimum temperature inside the cask is estimated to be 85°C, resulting in the measured water vapor corresponding to a RH of less than 10%. At 10% RH, there can be some (partial surface coverage / one molecule thick films) water adsorption on surfaces below about 120°C (at 2.2 bars).

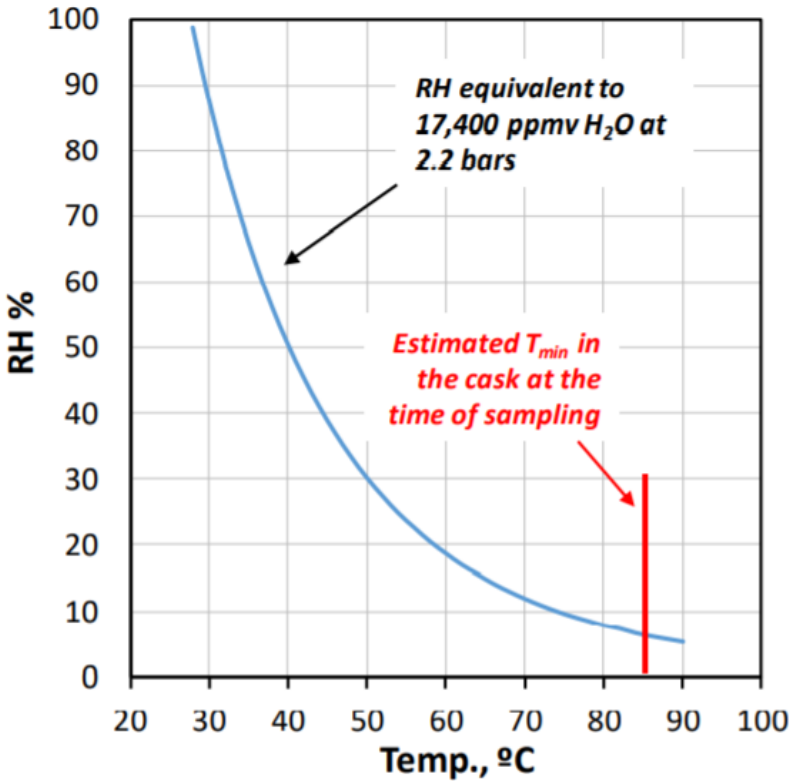


Figure 2-3. Water vapor / humidity levels inside the cask [Bryan, 2019a]

## 2.4. Physisorbed/Chemisorbed Water on Component Surfaces

The stored fuel and adjacent structures are relatively hot as shown in the temperature models, Figure 2-4 from [Fort, 2019]. Surface-adsorbed water can have varying adsorption energies, often with the first few monolayers strongly bound to the surface and additional, more weakly bound layers forming on top due to equilibrium with the humidity. Weakly physisorbed water is assumed to be present only on the cooler surfaces of the cask wall (i.e., on the steel liner) and assumed to be absent on the fuel surfaces due to the temperature and the drying procedures.

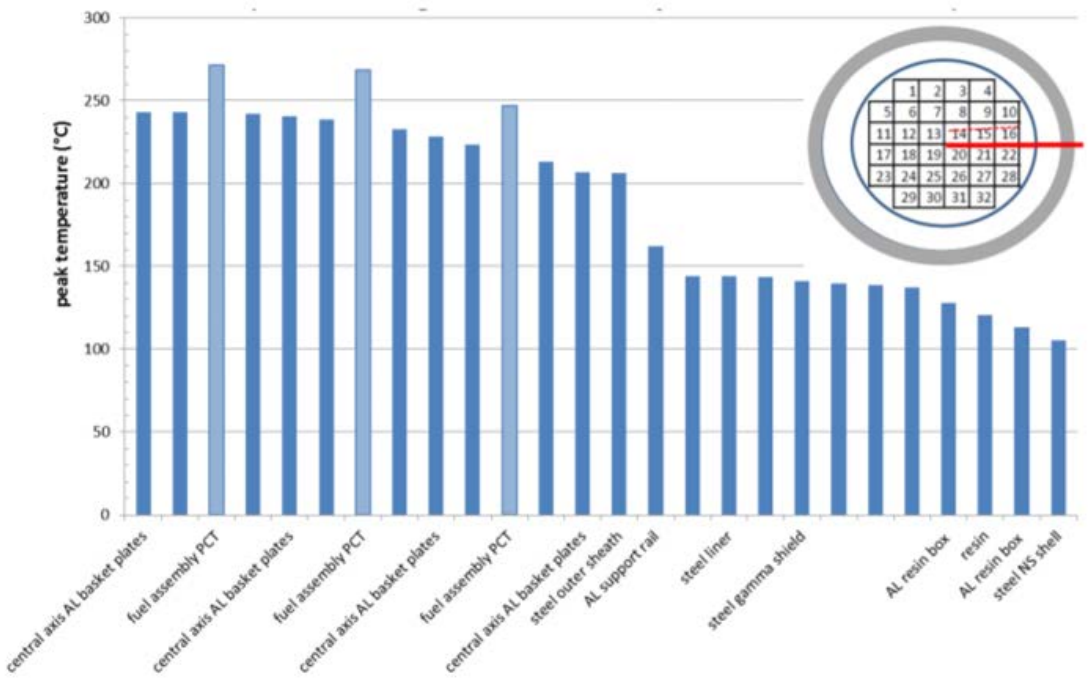


**Figure 2-4. Radial distribution of system component temperatures at the axial location of Peak Cladding Temperature for initial storage conditions (as of 7/31/2017) [Fort, 2009]**

In this study, "chemisorbed water" is strictly defined as the water that is incorporated chemically in hydrated oxides such as aluminum (oxy)hydroxides. This water can be present in the cask and associated hydrated surface oxides on the structural steel, fuel assembly components (primarily fuel rod oxides and crud), and in oxides on aluminum structures and neutron absorber plates (borated aluminum panels).

### 2.4.1. Stainless Steel

Per Dylla [Dylla, 2006], the strongly bonded physisorbed/chemisorbed water on stainless steel is less than a monolayer in thickness on an actual surface area basis, but is equivalent to about five monolayers when considering effective geometric surface area, as noted in Figure 2-5. Additional layers of physisorbed water are weakly bound and reported to easily desorb in vacuum and are thus expected to be absent everywhere but near the outer perimeter of the cask with the lowest temperatures.

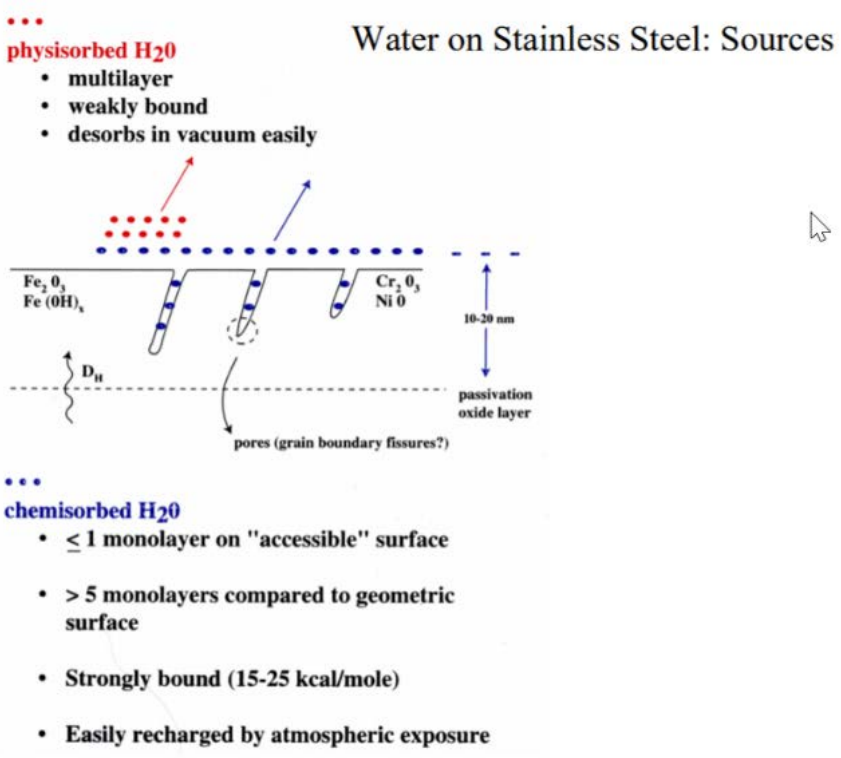


Figure 2-5. Schematic of adsorbed water on stainless steel [Dylla, 2006]

### 2.4.2. Fuel Assembly

There are primarily three sources of physisorbed/chemisorbed water on the fuel assemblies.

One source is the stainless-steel components (nozzles), but since these have relatively small surface areas and a low amount of physisorbed/chemisorbed water, these components are not included in the analysis.

Another possible source is $H_2O$ strongly bonded to the zirconium oxide on the surface of the fuel rods. The depth of any truly hydrated zirconium oxide, if present, is likely at most only a few molecular layers and is not representative of the bulk of the zirconium oxide. This source associated with adsorbed water on $ZrO_2$ will be discussed in more detail in the physisorbed/chemisorbed water section.

Crud is observed on some fuel rods. For PWR rods, the crud is generally black or shades of gray and consists of partially substituted nickel ferrite or spinel with (generalized) composition $Ni_xFe_{3-x}O_4$ (with x ranging from 0 to 1) [Hazelton, 1987]. Reference [Hazelton, 1987] provides a good historical crud review. Some crud contains oxyborates that have been associated with an axial offset anomaly. The presence of crud on fuel rods varies greatly between plants, between assemblies, between rods in assemblies, and axially along fuel rods. There are two general types of crud: flocculant (loosely adhering) and tenacious (denser and more strongly adherent). When present, the crud is observed at the hottest rod locations and typically not over the full rod length. Figure 2-6 is an example of rods with light to moderate crud and Figure 2-7 is a cross section of heavy crud showing the structure of internal boiling chimneys. It is difficult to directly measure crud thickness, but, if present, it can vary from <1 micron to >100 microns with a typical local maximum value of 1 to 20 microns. Figure 2-8 compares the eddy current oxide measurement with the metallographic sample measurements and indicates, for this example, that the crud thickness accounts for about 20 microns of the total eddy current “oxide” measurement at the high temperature locations.

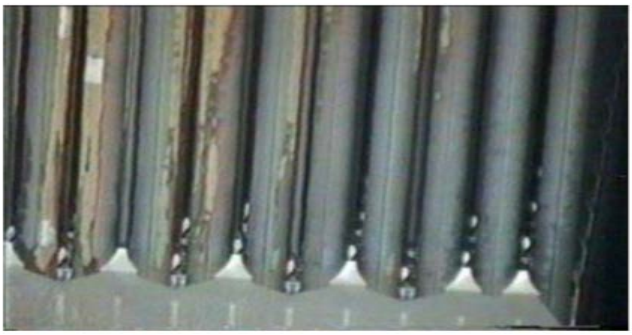

**Figure 2-6. Fuel rods with light-to-moderate crud [Knott, 2003]**

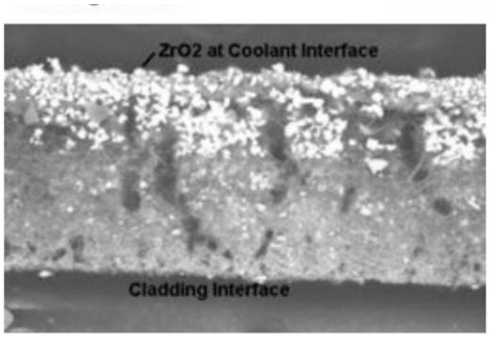


**Figure 2-7. Cross-section of heavy crud [Byers, 2010]**

CILC is another form of crud observed on some BWR fuel, but is not included in this study since no BWR rods are included in the HBU Demo from North Anna.

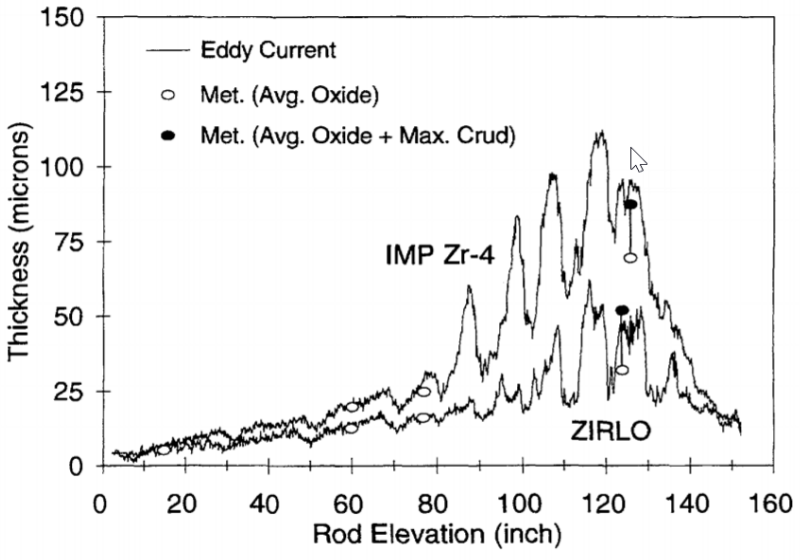


**Figure 2-8. Comparison of eddy current measurement of total "oxide" thickness to metallurgical measurements of crud and ZrO2 thickness [Wilson, 1999]**

### 2.4.3. Aluminum Alloys

There are two types of aluminum-containing components in the cask. One is the grid, used to facilitated heat transfer, that positions and supports the fuel assemblies, and the other is borated aluminum panels in the cells that serve as neutron absorbers. Unlike the steel and zirconium alloy components, which only have molecular-scale surface water films, aluminum can form (oxy)hydroxide or "hydrated oxide" films containing bonded hydrogen and oxygen in 2-to-1 ratio, i.e., chemisorbed water throughout the oxide. Radiolysis occurring due to the radiation field within the cask will interact with the oxide, and through radiolysis, hydrogen will be generated along with other related radiolysis species.

## 2.5. Water Retained in Pores and Fissures

While in the fuel pool, the fuel rods will retain water in oxide fissures and crud pores. Depending on the effectiveness of the drying operation during cask preparation for dry storage, some of this water/steam may remain in the structures. This water can contribute to moisture levels within the cask and produce hydrogen and other species with radiolysis.

Montgomery [Montgomery, 2018] summarizes the visual observations made on the sister rods of the rods loaded in the Demo. Figure 2-9, Figure 2-10, and Figure 2-11 show examples of the rod oxide appearance. Each figure is a montage of photos taken at intervals around the rod circumference and present a flattened view of a rod surface. Figure 2-11 shows crud examples. Pertinent observations on the crud and oxide are:

A. The M5® rod surfaces show a black pre-transition oxide. No significant fissures (or retained water) is expected to be present in this oxide.

B. The ZIRLO® rod surfaces show a moderate to heavy oxide. It is known that the heavier oxides are located at the higher duty areas of the rod near the top. For these rods, there can be some oxide fissures for water retention.

C. The Zirc-4 rods have the heaviest oxide and show signs of oxide spalling. These rods will have oxide fissures in the area of the moderate to heavy oxides. (There is only one Zirc-4 assembly and one low-Sn Zirc-4 assembly in the HBU cask)

D. Crud was observed on several rods. The crud appears to be tenacious and not flocculant. Flocculant crud, if originally present, was probably dislodged during pool storage and assembly movement. Crud itself is anhydrous, but the observed crud provides a potential source for retained water via pores and capillary forces.

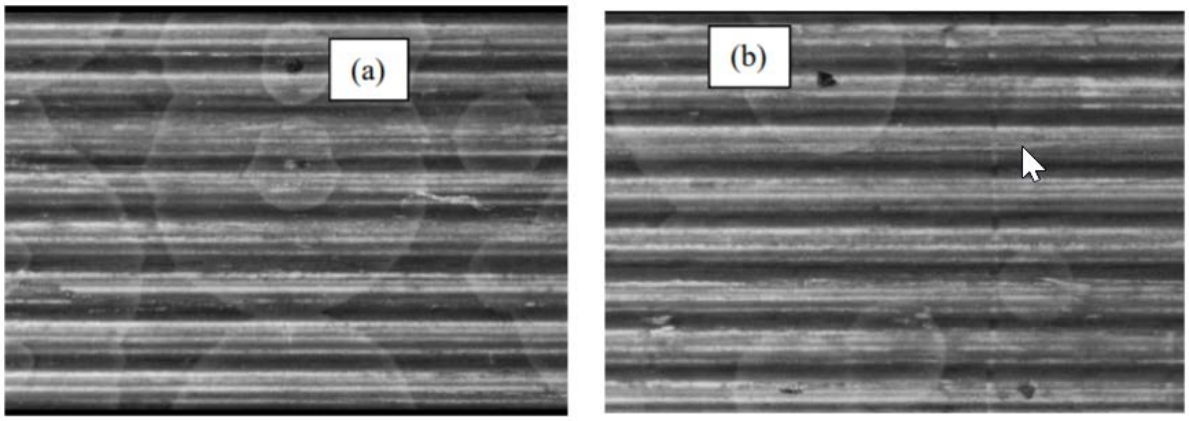


**Figure 2-9. Surface appearance at two M5 rod locations [Montgomery, 2018]**

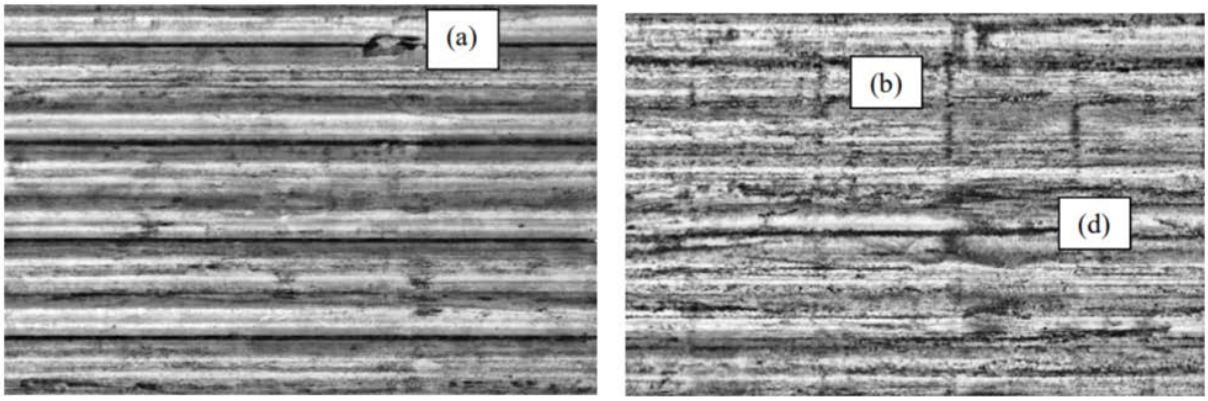


**Figure 2-10. Surface appearance at two ZIRLO rod locations [Montgomery, 2018]**

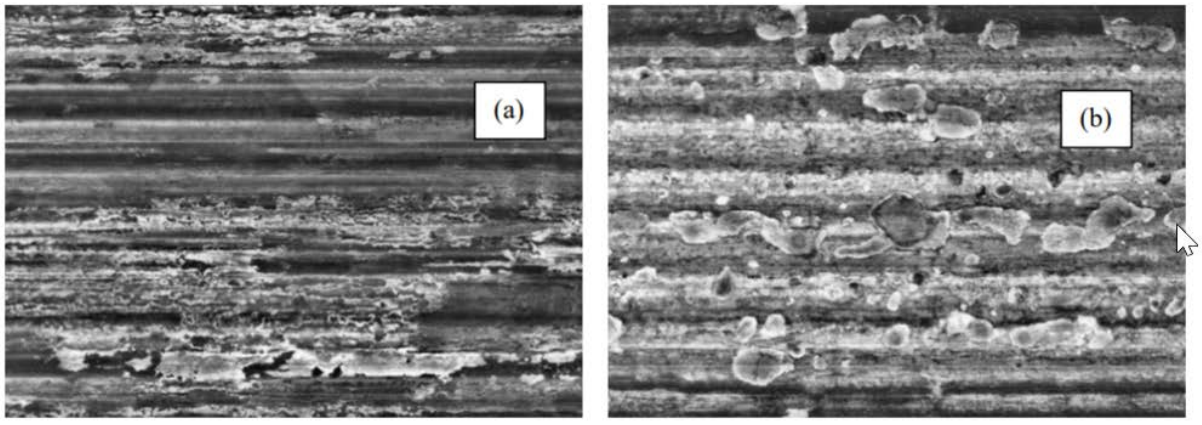


**Figure 2-11. Examples of observed crud; (a) is noted as a thin peeling crud and (b) is a heavier flaky deposit on top of a thick oxide [Montgomery, 2018]**

# 3. PHYSISORBED/CHEMISORBED AND PORE-RETAINED WATER SOURCES

## 3.1. Weakly Physisorbed Water on Component Surfaces

The peak stored fuel and adjacent structures are near 200°C during cask drying per Figure 2-4, and most weakly physisorbed water is therefore assumed to be desorbed and not present on the fuel rod and cell surfaces. Weakly physisorbed water is assumed to be present only on the cooler surfaces of the (steel) cask liner, and, given the estimated >3% humidity level in the cask at the 12-day sampling time, the weakly physisorbed water would be only a partial coverage of a molecule-thin film. The mass of a single-molecule-thick physisorbed water layer is reported to be between 0.187 and 0.3 mg/m$^2$ [Petrik, 2001; Wertsching, 2007]. A value of 0.3 mg/m$^2$ is used in this evaluation.

Steel is also present as liner in the cell network. After high-temperature drying, it is assumed that this steel remains hot (~150°C) and does not contain significant weakly physisorbed water, only the more strongly bonded physisorbed/chemisorbed water.

The reported cask pressure is 2.2 bar or 32 psi, and the water-saturated steam temperature point for this pressure is 123°C. Based on Figure 2-4, most of the component area is above this temperature, so a 25% surface area coverage is used for determining sensitivity to the water/hydrogen source from the steel surface weakly physisorbed water (on the steel liner only). If significant, the area and temperatures could be further evaluated.

## 3.2. Strongly Physisorbed/Chemisorbed Surface Water

The primary potential strongly physisorbed/chemisorbed water sources in the HBU Demo cask are from the oxides on the aluminum surfaces (structural and borated aluminum neutron absorbers), the fuel rod surface oxide, crud, and the steel surfaces. This section presents a summary evaluation of each of these sources regarding potential quantities of equivalent water mass retained. Where detailed component data was not found, estimates are made regarding dimensions. While exact quantification is unavailable and estimates are used, the relative water quantities can be estimated, and a qualitative determination made of the source's relative significance.

For the cask system, the strongly physisorbed/chemisorbed water for steels and zirconium oxide refers to molecularly thin surface layers of $H_2O$ that are bonded via surface radicals and/or a very thin layer of hydrated oxide. For other materials, such as aluminum, chemisorbed refers to the water/hydroxyls chemically incorporated within and throughout the oxide structure to form (oxy)hydroxides.

### 3.2.1. Aluminum Alloy Structural Components

Much of the aluminum alloy surface is contained in the basket cell matrix. However, the basket is constructed so that the aluminum in the cell matrix is sandwiched between stainless-steel plates. Per reference [Fort, 2019], "the basket cells are formed […] with stainless-steel sheets on the outer faces of the basket structure. Much thicker aluminum alloy plates are sandwiched between the stainless-steel plates, with double-thickness aluminum plates forming the central 'cross' of the basket". Assuming these layered structures are tightly fastened together, the exposed faces of the basket cell matrix should be stainless steel with minimal, if any, exposure of the aluminum plate faces.

The supporting rails between the cell matrix and the cylindrical walls of the cask are also made of aluminum, which is exposed to the cask environment.

The exposed aluminum surfaces may have hydrated oxide (aluminum (oxy)hydroxide) formed from ambient exposure and potentially additional oxide formed during the initial stages of high-temperature drying if sufficient water vapor is present. At low temperatures, primarily trihydroxides ($Al(OH)_3$ or

$Al_2O_3 \cdot 3H_2O$), i.e., gibbsite or bayerite, would form, but depending on the thermal exposure during drying, the gibbsite may thermally decompose to boehmite (AlOOH or $Al_2O_3 \cdot H_2O$). Based on the molecular weights, about 34.6% ($M_{3(H2O)}/M_{Al2O3 \cdot 3(H2O)}$=54/156) of the bayerite/gibbsite mass is water and 15.0% ($M_{H2O}/M_{Al2O3 \cdot H2O}$=18/120) of the boehmite mass is water. The surface (oxy)hydroxides contain chemisorbed water that is not expected to be totally removed during the cask drying and is considered a source for $H_2$ from radiolysis during storage. It is evaluated in a subsequent section of this report that quantifies radiolysis sources. Bayerite films approximately 8 microns thick have been observed on aluminum after 36 days immersion in room-temperature liquid water [d'Entremont, 2020]. This analysis will assume 8 microns of bayerite as a starting point, which is expected to be conservative since the rails are not expected to have a significant history of immersion in water other than the cask loading process. If thermally decomposed to boehmite during drying, the 8 microns of bayerite would result in ~5.2 microns of boehmite, assuming negligible spalling.

### 3.2.2. Borated Absorber Panels

The borated absorber panels are incorporated into the basket, according to the description in Fort et al. [Fort, 2019], and are sandwiched between other aluminum plates and stainless-steel plates. As discussed above for the structural aluminum plates in the cell matrix, it is assumed that the surfaces of the borated absorber panels are not exposed.

### 3.2.3. Fuel Oxide

There are two potential areas for retained water in the fuel rod surface oxide. One is molecular water films physisorbed/chemisorbed on the surface, and the other is retained water in the oxide fissures. Typically, oxides over about 40 microns in thickness contain fissures in the structure that can contain residual water. It is expected that some of this water will be vaporized and escape during the heated drying operation. The water retention could be better quantified with testing of discharged rod sections with thick oxides.

Many investigators [Agayev, 2017; Skotnicki, 2015; Petrik, 2001; Holmes, 1974; Köck, 2016; for example] have evaluated the strong physisorption/chemisorption of water on $ZrO_2$ using powders, thin lab-grown oxides, and some with added solutions for scavenging radiolysis species. It is reported that hydroxyls are formed at the oxide surface when water is present, and these hydroxyls act as anchors for one or a few molecular layers of adsorbed water. It should be emphasized that this is a surface effect that does not involve chemically incorporated water throughout the bulk of the oxide, unlike the chemisorbed water associated with aluminum alloys. Thus, the adsorbed water source is relatively limited even with the large rod surface area. Bryan [Bryan et al., 2019b] estimates the physisorbed/chemisorbed water on the fuel rod oxide surface to be about 12 mg per assembly. In this evaluation, we find a value of about 10 mg of physisorbed/chemisorbed water per assembly with a single water layer. However, for the base calculations, we include 3 water layers. The rate of water removal with cask drying procedures is not known, although it is speculated that some physisorbed/chemisorbed water will be removed with drying. The contribution to the radiolytic $H_2$ generation from fuel rod surfaces is included in the hydrogen generation evaluations.

### 3.2.4. Fuel Rod Crud

Crud consists of anhydrous compounds and is considered for this evaluation to not include chemisorbed water, although there is probably some small amount of molecular-thin chemisorbed water film on the particles. The bulk of water source associated with crud is related to the porosity and is included in the physisorbed / pore water section.

### 3.2.5. Steel Surfaces

The steel surfaces in the cell matrix and the surrounding liner and cask wall will initially have some surface strongly physisorbed/chemisorbed water. Per Dylla [Dylla, 2006], the strongly physisorbed/chemisorbed water on steel comprises less than a monolayer on the actual surface area but is equivalent to about five monolayers when considering the nominal/macroscopic surface area. The factor of five for actual versus macroscopic surface area appears to be very conservative based on an effective surface macro versus micro increase for zircaloy cladding of less than 10% [Bryan et al., 2019b]. It is expected that at least some of this steel surface adsorbed water will be depleted during the drying operation. For the evaluation, a conservative five layers of strongly physisorbed/chemisorbed water will be used for the base source calculation.

## 3.3. Pore-Retained Water

As previously discussed, water can be retained in the pore structure of the crud and in oxide fissures. While failed fuel is another potential water source, the Demo cask does not include failed fuel, and a failed fuel source is not included in this evaluation. The pores and fissures in the fuel oxide are heated during the drying operation, and the majority of water initially present from the fuel pool exposure is expected to be vaporized and purged from the oxide, similar to the crud discussion below.

### 3.3.1. Crud

The crud level and type vary greatly with the different fuel operating conditions. Crud, if present, generally accumulates on the upper portions that have high temperature/high heat transfer operation. Also, during storage in the fuel pool, the loose crud tends to flake off and settle in the bottom of the pool, so the crud present at the time of dry storage is highly likely to have reduced surface coverage and mass compared to when the fuel is first moved to the fuel pool.

Weakly physisorbed water and weakly-bound pore-related water are assumed to be removed from the crud during drying. The crud is attached to the rod surface, and it is postulated that the crud will be heated sufficiently during drying to convert any retained water to steam and release it. However, the crud does impact the effective surface area of the fuel rods.

### 3.3.2. Fuel Rod Oxide

Similar to the above crud review, water that originally existed in the oxide fissures is assumed to be removed with the drying operation. Significant water re-adsorption will not occur subsequent to the drying because of the high rod surface oxide temperatures and low RH. There is an effective surface area increase with oxide fissures and crud flaking which relates to surface physisorption/chemisorption. Crud and oxide fissures are addressed in the water source calculations.

# 4. EVALUATION OF WATER AND ASSOCIATED HYDROGEN CONTAINED IN ALL COMPONENT SOURCES

The initial water inventory associated with various cask components after drying and the total potential hydrogen that could be released from these water sources are estimated. The hydrogen source is assumed to be from radiolysis of the water sources only (i.e. generation of hydrogen via corrosion is assumed to be insignificant). The water sources include the water inventory of all components, whether chemisorbed, physisorbed, or in pores and fissures. A major assumption in this work is the remaining water associated with the component surfaces, as physisorbed/chemisorbed or in pores in attendant films (e.g. crud on the fuel) following the drying operation.

In the evaluation of the structural components in the cell matrix, we assume that 1) the aluminum structural plates do not have significant water exposure prior to assembly (and thus do not have significant loading of (oxy)hydroxides) and 2) the stacked plates in the cell matrix are firmly sandwiched between the exterior stainless steel plates such that the interior faces are inaccessible to water once assembled. As a result, the surface area of the interior faces of the plates in the cell matrix are neglected in the main calculation of water sources: this includes both faces of the structural aluminum plates in the cell matrix, both faces of the borated neutron absorbers, and the back face of the stainless steel plates. A separate calculation of water associated with the aluminum plates in the cell matrix is performed to estimate the additional source if these surfaces did participate.

## 4.1. Steel Structurals

As previously estimated, the nominal exposed stainless-steel surface area is about 27.5 $m^2$ for the cask liner plus 115.0 $m^2$ for the cell matrix for a total of 142.5 $m^2$, plus we add 10% for effective surface area. It is conservatively assumed that there are five monolayers of strongly physisorbed/chemisorbed water on the steel surface. In addition, 25% of the cask inner surface is assumed to have one layer of weakly physisorbed water (conservative, since at the cask humidity there is typically less than a monolayer coverage predicted).

The strongly physisorbed/chemisorbed water inventory for the steel components is calculated by multiplying the total effective surface area by the chemisorbed water loading, i.e., $1.1(142.5\ \mathrm{m^2})(5\ \mathrm{monolayers})(0.3\ \mathrm{mg/m^2/monolayer}) = 235.1\ \mathrm{mg}$ or 0.01306 mol $H_2O$. If all of this $H_2O$ produced molecular $H_2$ under irradiation, then dividing 0.01306 mol $H_2$ by the estimated 386 mol He (Section 2.1.5) estimates 33.8 ppmv $H_2$ contributed by water strongly physisorbed/chemisorbed on steel. A similar calculation for 0.25 monolayers of weakly physisorbed water on only the cask liner area yields 2.272 mg / $1.26\times10^{-4}$ mol $H_2O$, contributing a maximum of 0.327 ppmv $H_2$.

## 4.2. Aluminum Structures

The chemisorbed water related to the aluminum structures is an integral part of surface (oxy)hydroxides, which can form under exposure to liquid water or water vapor. Gibbsite/bayerite, $Al(OH)_3$ or $Al_2O_3{\cdot}3H_2O$, forms under low-temperature water exposure and may remain if it does not reach around 200°C during drying, e.g., possibly in the cooler regions around the cask edges. Boehmite, AlOOH or $Al_2O_3{\cdot}H_2O$, is the oxide expected on the aluminum surfaces after high-temperature drying. These (oxy)hydroxides provide a source for $H_2$ that can be released with radiolysis. Note that $Al_2O_3$, which forms a thin layer almost instantly on aluminum exposed to air, contains no hydrogen, so aluminum exposed only to dry air would not provide a hydrogen source. The radiolysis release rate will be discussed in a later section.

In this section, as a worst case scenario, the total water/hydrogen reservoir associated with the aluminum (oxy)hydroxides is calculated. The calculation involves determining the total (oxy)hydroxide mass based

on the assumed oxide thickness, the surface area covered, and the (oxy)hydroxide density (2.53 g/cm$^3$ for bayerite and 3.01 g/cm$^3$ for boehmite [Wefers, 1987]); calculating the mass of chemisorbed water in the oxide based on the mass percentage (34.6% for bayerite and 15.0% for boehmite); using the molar mass of water to convert the mass to moles of $H_2O$, which is equal to the maximum possible moles of $H_2$ that can be released, and determining the maximum ppmv of $H_2$ released by dividing by the amount of cask gas.

### 4.2.1. Aluminum Rails

For the aluminum rails, the estimated surface area is 86.29 m$^2$ (Section 2.1.3).

Assuming 8 μm thick film of bayerite remaining as bayerite after drying, the mass of oxide is about 1750 g, containing 605 g or 33.6 mol $H_2O$. Dividing 33.6 mol $H_2$ by the estimated 386 mol He yields 8.69% or $8.69\times10^4$ ppmv from bayerite.

Alternatively, assuming 5.2 μm of boehmite (corresponding to complete drying of 8 μm bayerite), the mass of oxide is about 1340 g, containing 202 g or 11.2 mol $H_2O$. Dividing by the estimated 386 mol He yields 2.90% or $2.90\times10^4$ ppmv $H_2$ from boehmite.

This hydrogen is contained in the oxide structure, but some will be released during radiolysis. This calculation indicates that the aluminum (oxy)hydroxides in the rails provide a significant potential source for hydrogen. It is chemically bonded and not readily released. Interaction with the radiation field present in the cask during storage is known to break these bonds, and some hydrogen will be generated and released over time. The release rate is discussed in the radiolysis analysis section.

### 4.2.2. Aluminum Cell Matrix Plates

Only if the interior aluminum plates remain accessible to water and thus have a loading of (oxy)hydroxide and participate in radiolytic release of hydrogen, they could serve as a significant additional source of $H_2$. The surface area for the set of structural aluminum plates in the cell matrix and the set of borated aluminum plates is estimated to be 126 m$^2$ each for a total of 253 m$^2$. Following the same basic procedure as for the rails, the estimated water content is 1770 g / 98.4 mol $H_2O$ assuming bayerite and 591 g / 32.8 mol $H_2O$ assuming boehmite. The maximum $H_2$ generated from this amount of (oxy)hydroxide would be 25.5% / $2.55\times10^5$ ppmv and 8.5% / $8.5\times10^4$ ppmv for bayerite and boehmite, respectively.

## 4.3. Fuel Rods and Other Zr Components

The evaluation of water/hydrogen sources on fuel rods includes strongly physisorbed/chemisorbed water on oxide and capillary water associated with oxide fissures and crud pores.

### 4.3.1. Surface Physisorbed/Chemisorbed Water on Fuel Rod Surface

Studies [Koch, 2016; Hou, 2016] have shown that the $ZrO_2$ surface can effectively chemically bond water molecules via surface hydroxyls. This is a strongly physisorbed water source as a crystallographic hydrated oxide is not produced. This physisorbed/chemisorbed water is a few molecular layers thick [Bryan, 2019b], and some amount may be removed during drying. To estimate the quantity of water/hydrogen from this source, a three-molecule-thick layer of water is assumed to be present after drying. This water is limited to the surface of the $ZrO_2$ rather than chemically incorporated into the bulk of the oxide.

It is assumed that the hydrogen contained in the strongly physisorbed/chemisorbed water would only be released with radiolysis as discussed in the Radiolysis section.

### 4.3.2. Oxide Fissures and Flaking

Information on oxide fissures and flaking morphology is qualitative, and there is no applicable quantitative data found to allow an accurate assessment of this impact. Oxide fissures and flaking will vary between and within rods depending primarily on the amount of local corrosion. Typically, the thicker oxides are present on about 1/3 of the axial rod length at spans near the top. The different corrosion rates between the M5, ZIRLO, and Zirc-4 rods indicate that the M5 rods (56% of rods in the Demo) have lower oxide thickness and probably do not have oxide fissures or flaking. The ZIRLO rods (38% of rods) have thicker oxides and are assumed to have minor fissuring. The Zirc-4 rods (6% of Demo) show visual signs of flaking (and fissures by association). For this sensitivity evaluation, a water/hydrogen quantity equal to the nominal surface water is included.

### 4.3.3. Crud

The crud can have >50% porosity. Unlike the aluminum (oxy)hydroxides, the crud is anhydrous, so the main potential for retained water is associated with the crud porosity. It is postulated that the majority of the water entrained in the crud will be removed by the dry gas purge and the vacuum evaporation and that the crud temperature will be similar to the fuel rod temperature, precluding water re-condensing. One approach to estimate the equivalent water retained in the crud is to assume that the free water was removed during drying and the porosity in the hot crud is now in equilibrium with the water vapor in the cask. With this assumption, it can be concluded that the water vapor in the crud does not have a significant impact on the total water inventory in the cask. For this sensitivity evaluation, it is assumed that the crud effectively doubles the rod surface area and contributes an amount of hydrogen equivalent to the nominal $ZrO_2$ physisorbed/chemisorbed source. When additional information is available on the sister rod examination and data on drying impacts on retained water, a better crud impact evaluation can be made.

### 4.3.4. Total Water Content Associated with Zr Surfaces

The total nominal area of all fuel rods was estimated to be 978 $m^2$. Adding the 37% surface area for additional Zr components gives a total $ZrO_2$ surface area of 1340 $m^2$. Accounting for three monolayers of water at 0.3 $mg/m^2$/monolayer and multiplying by a factor of three to account for the oxide fissures and crud, the total mass of water is estimated as 3.62 g or 0.201 mol $H_2O$ (0.147 mol on the fuel rods and 0.0543 mol on the additional Zr components). Dividing 0.201 mol $H_2$ by the 386 mol He estimates the maximum $H_2$ yield from physisorbed/chemisorbed water on $ZrO_2$ as 520.3 ppmv.

## 4.4. Water Vapor

In reference [Bryan, 2019a], it is reported that at 12 days after Demo cask drying and sealing, the cask atmosphere at 2.2 bar contained about 17400 ppmv water vapor. This water vapor content represents less than 3% RH when extrapolated to a cask gas temperature of 140°C [Poloski, 2019].

Assuming 20000 ppmv initial water vapor as a conservative estimate, with the estimated 386 mol He, this would correspond to a water inventory of about 7.7 mol $H_2O$. It is recognized this value is a factor of ~10 greater than that corresponding to the 3 torr condition for vacuum drying. The contribution of water vapor on radiolysis is discussed in the section on Radiolysis.

# 5. RADIOLYSIS OF WATER SOURCES AND HYDROGEN GENERATION

The focus of this section is to evaluate the potential hydrogen generation with radiolysis of the water sources in the cask after drying and closure. There are a number of parameters that are not well quantified, and corresponding assumptions have been made and documented. The primary value of this evaluation is the determination of the relative hydrogen generation from the various sources and their sensitivities to parameter ranges. Gettering of hydrogen by reactions with the fuel clad and other zirconium alloys is not included. Chemical back reactions were neglected.

## 5.1. $G_{H2}$ Values

$G_{H2}$ represents the production rate of hydrogen molecules during radiolysis of hydrogen-containing materials. $G_{H2}$ values vary greatly depending on the material being irradiated, the environmental parameters, and the radiation characteristics.

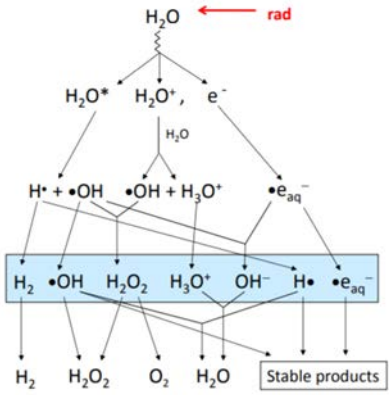


**Figure 5-1 Schematic of the evolution of water radiolysis products [Yousefi thesis]**

The gamma radiolysis of $H_2O$ has been studied extensively. The radiolysis results in the rapid formation of molecules, atoms, ions, and radicals. These products react and form stable components ($H_2$, $H_2O_2$, and $H_2O$), as shown in Figure 5-1. The rates of production by radiolysis are designated by the G-value, which is reported in units of molecules, ions, or radicals (depending on the product) per radiation dose. For $H_2$, $G_{H2}$ is reported in molecules of $H_2$ per 100 eV or in μmol $H_2$ per joule (1 μmol/joule = 9.63 molecules/100 eV). The relative quantities of the stable components and the resulting calculated G are dependent on the characteristics of the system/environment in which they are being produced and are not constant values across differing systems.

The factors that affect G-values have different impacts depending on the species being measured. A focus of this evaluation is to examine the production of hydrogen inside the demo storage container for spent nuclear fuel (SNF); thus, the discussion of G-values will be directed mainly to the impact on $H_2$ production.

### 5.1.1. Temperature

Elliot [Elliot, 2009] summarized data regarding the effect of temperature on $G_{H2}$ from several literature sources. The summary is shown in Figure 5-2 and indicates an increasing $G_{H2}$ with temperature. Some of the data points were generated in water with added solutions which can impact the G value by scavenging and reacting with other species from the radiolysis. The trend line follows the data that was extrapolated

to zero concentration and is consistent with the typical $G_{H2}$ value from Spinks of 0.45 molecules/100 eV. The trend line follows equation {1} and has a $G_{H2}$ value of 0.44 molecules/100 eV at 23°C and 0.56 molecules/100 eV at 250°C for the system that was used to determine the values. The temperatures within the fuel element storage cask vary and will decrease over time but, based on the data in Figure 5-2, the $G_{H2}$ value in the cask is expected to have relatively small temperature-related variation and is expected to remain below 0.6 molecules/100 eV for the storage conditions.

$$G_{H2} = 0.419 + 8.721\times10^{-4}\ T - 4.971\times10^{-6}\ T^2 + 1.503\times10^{-8}\ T^3 \qquad \{1\}$$

where T is the temperature in °C and $G_{H2}$ is given in molecules/100 eV.

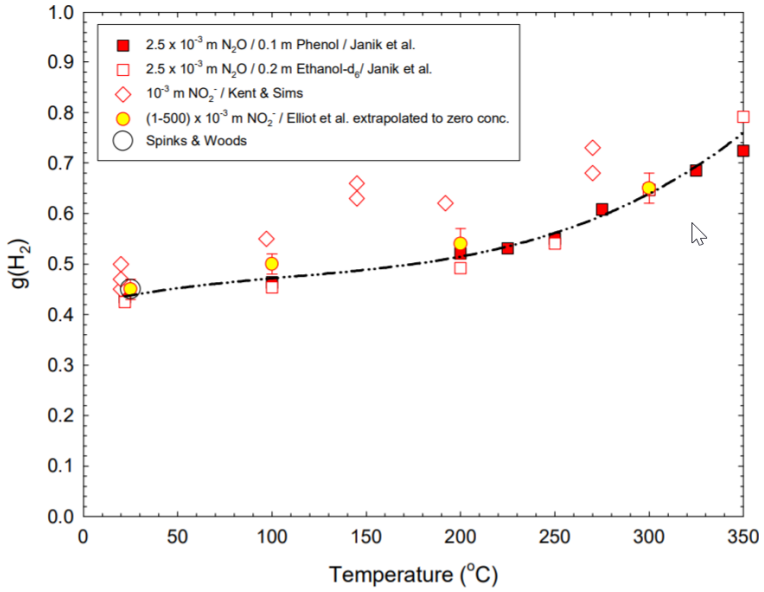


**Figure 5-2. Temperature Effect on $G_{H2}$ [Elliot, 2009]**

### 5.1.2. System Environment

The system environment, cover gas or liquid solutions, will affect the amount of free hydrogen generated in the system and also the calculated G-value. The presence of scavenger species can affect the hydrogen production by interfering with precursor radicals produced in the radiolysis. Figure 5-3 from Horne [Horne, 2017] demonstrates that the presence of $NaNO_3$ suppresses the generation of hydrogen gas, which was attributed to quenching of excited water molecules via a process involving $NO_3^-$, while Figure 5-4 from [Boyd, 1973] is an example of the varying G-values of mixtures of HCl (a source for hydrogen) and water, where the production of hydrogen is increased by the presence of another hydrogen source in addition to the water vapor. For the evaluation of hydrogen generation in the SNF cask, the environment is relatively pure with only helium cover gas, so there should be no significant impact on the $G_{H2}$ values due to reactions with the cask gas environment (except for possible minor effects from small amounts of residual air and hydrocarbons). However, the environmental impacts on reported $G_{H2}$ values in the literature need to be evaluated to assess their applicability to applications where pure water or water vapor are being considered since the G-value is system environment dependent.

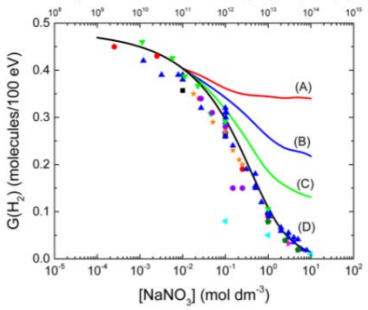


**Figure 5-3 $G_{H2}$ as a function of $NO_3^-$ concentration. [Horne, 2017]**

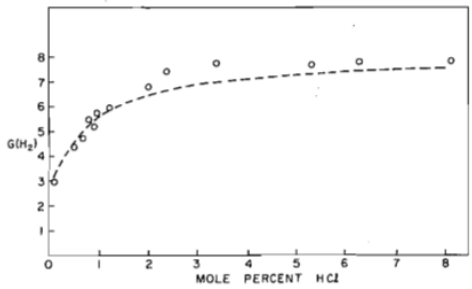


**Figure 5-4. Effect of water vapor-HCl mixtures on $G_{H2}$ [Boyd, 1973]**

### 5.1.3. Alloy Surface and Substrate

Elliott [Elliott, 2009], discussing radiolysis of physisorbed and chemisorbed water, reported that the substrate where the water is adsorbed or retained as radicals has an impact on the hydrogen production rate and corresponding G-values. Westbrook [Westbrook et al, 2015] reported that two different aluminum (oxy)hydroxides, boehmite and gibbsite, produce hydrogen at different rates under gamma radiation. La Verne [La Verne, 2009] reports different hydrogen production rates for powdered oxides of U, Zr, and Ce. For the evaluation of radiolysis in storage casks, the primary surfaces are the zirconium-alloy fuel rods with an oxide surface that was grown during operation, steel structural components, and aluminum structural rails.

When evaluating representative G-values, the substrate morphology also needs to be considered. For example, a significant portion of the G studies reported in the literature are based on using oxide powders, powder-compacted pellets, or thin lab-grown oxides. The powder/thin oxide structure, porosity, and surface area can differ widely from the morphology of operationally grown oxides on base metal surfaces and lacks applicable SNF metal-substrate-related effects.

There have been numerous reports on radiolysis of water in contact with $ZrO_2$ powders and crystals and evaluations of the effects of surface physisorbed/chemisorbed water. Garibov [Garibov et al., 2015] reports a $G_{H2}$ value of 2.14 molecules/100 eV for adsorbed water on nano-$ZrO_2$ powder at a temperature of 300 K (with increasing G-value as the temperature increased). Petrik et al. [Petrik et al., 2001] also observed high G-values for water adsorbed on $ZrO_2$ powders compared to pure water. However, they also studied $ZrO_2$ doped with $Nb^{+5}$ and with $Li^+$ or $Rb^+$, and for the $ZrO_2$ powders doped with $Nb^{+5}$, the hydrogen production was significantly reduced as shown in Figure 5-5 [Petrik et al., 2001]. Doping the $ZrO_2$ powders with $Li^+$ or $Rb^+$ increased the radiolytic $H_2$ yield by a factor of 2 at 0.1% mass of the dopant [Petrik et al., 2001], so the presence of dopants can either suppress or enhance $H_2$ production depending on the dopant. It was postulated that the defects in the oxide crystal lattice is an important factor impacting water radiolysis occurring on $ZrO_2$ surfaces. It is important to note that most, if not all, of the $ZrO_2$ radiolysis studies use very pure material: fine powders, crystals, or very thin lab-grown oxides

with no Nb or other alloying elements present. Since the clad on the ZIRLO and M5 rods have 1% Nb as an alloying additive, the resulting oxide will also contain Nb along with other precipitates that produce lattice defects. While the two Zirc-4 assemblies do not have Nb in the cladding alloy, they do have Sn, Cr, and Fe which will also result in lattice defects. It is assumed that the 7% of rods in the cask will have similar radiolytic surface characteristics as the Nb containing rods. Based on these observations, the $G_{H2}$ value used in this study for the fuel rod oxide is the value observed for typical water radiolysis of 0.47 molecules/100 eV, i.e., neglecting any potential enhancement due to the presence of the $ZrO_2$ surface or suppression due to the Nb content.

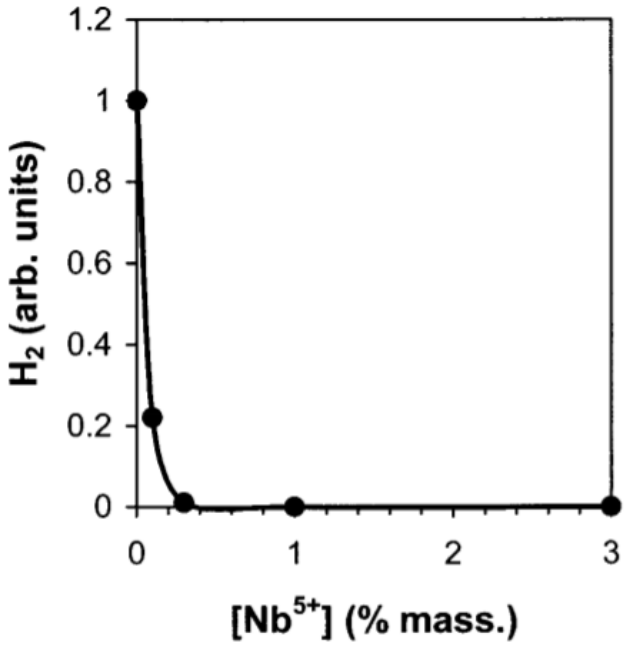


**Figure 5-5. Effect of $Nb^{+5}$ doping of $ZrO_2$ on the radiolytic $H_2$ production from adsorbed water [Petrik et al., 2001]**

Kaddissy [Kaddissy, 2016] and Westbrook [Westbrook et al., 2015] both studied the radiolytic hydrogen production from gamma irradiation of hydrated aluminum oxides. $G_{H2}$ results are summarized in Table 5-1 for $Al(OH)_3$ powders and for small and large AlOOH powders. The larger powder size is more analogous to the oxide films grown on aluminum surfaces, and $G_{H2}$ reported for the larger boehmite powders ranged from 0.048 to 0.13 molecules/100 eV, i.e., roughly one tenth to one quarter of the typical reported $G_{H2}$ for water. For this evaluation, $G_{H2}$ values of 0.05 and 0.02 molecules/100 eV are used for the boehmite and bayerite calculations, respectively.

**Table 5-1. $G_{H2}$ measured for various $Al(OH)_3$ and AlOOH powders from two studies. Values for "large" boehmite powder ranged from 0.048 to 0.13 molecules/100 eV [Kaddissy, 2016].**

| Material | $G(H_2)$ (mol/J) × $10^{-8}$ | $G(H_2)$ (molecules/100 eV) | Reference |
|---|---|---|---|
| AlOOH (large) | 0.57-1.3 | 0.055-0.13 | [Westbrook, 2015] |
| AlOOH (large) | 0.5 ± 0.2 | 0.048 ± 0.02 | [Kaddissy, 2016] |
| $Al(OH)_3$ | 0.21 ± 0.05 | 0.020 ± 0.005 | [Kaddissy, 2016] |
| AlOOH (small) | 0.04 ± 0.02 | 0.004 ± 0.002 | [Kaddissy, 2016] |
| $Al(OH)_3$ | Low, not evaluated | Low, not evaluated | [Westbrook, 2015] |

### 5.1.4. Gamma Dose and Initial Transition Effects

The long-term, steady-state G-values are critical data when evaluating water radiolysis in dry storage systems. The G-values calculated from initial irradiation doses can be/are different than the long-term doses when a quasi-steady-state condition evolves including back reactions and environmental effects. An example of this is shown in Figure 5-6 with measurements of Arkhipov [Arkhipov, 2007], where G-values were measured in water vapor for different accumulated doses and radiation dose rates. Initially, the calculated $G_{H2}$ values are high—close to 9 molecules/100 eV, but as the dose accumulates over time, the G-value decreases. To obtain an estimate of the longer time/dose G-value, a set of representative points was obtained from the graph and are listed in Table 5-2. These data points are plotted in Figure 5-7 and indicate that the G-value is not affected by the range in dose rates, Gy/s, but is instead only a function of the total accumulated dose. The trend line for the curve was calculated to be $G_{H2}$ = (22.793 molecules $kGy^{0.568}$/100 eV)$(dose)^{-0.568}$ and suggests an asymptotic approach to a steady state G-value. Extrapolating the fit to a dose of 1000 kGy predicts a value of $G_{H2}$ = 0.45 molecules/100 eV. This value is in the same range as typically used for $H_2$ yield from water and emphases the risk of using low-dose G-values for longer-term (quasi-steady-state) calculations.

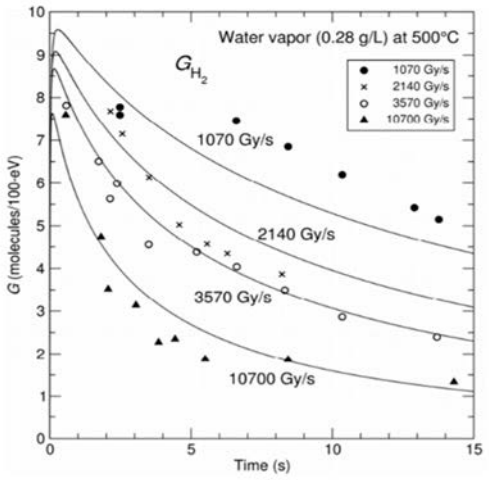


**Figure 5-6. Hydrogen yield over time for water vapor for various radiation dose rates [Wittman, 2013]**

In addition to the total dose/steady state influence on G, the radiation energy level can affect the measured G-value [Le Caër, 2011; Kabakchi et al., 2013; Wang, 2013]. Wang's [Wang, 2013] summary of G-values reported by researchers incorporating different radiation energies is shown in Table 5-3. Here, the value of $G_{H2}$ ranged from 0.45 to 1.8 molecules/100 eV depending on the energy of the radiation. The lower-LET gamma ray energy is applicable to the current evaluation.

**Table 5-2. Selected data points from Figure 6-6 for replotting**

| Gy/sec | Time seconds | kGy - total | $G_{H2}$ |
|---|---|---|---|
| 1070 | 14 | 15 | 5.1 |
| 1070 | 6.5 | 7 | 7.5 |
| 1070 | 8.5 | 9 | 7 |
| 3570 | 14 | 50 | 2.4 |
| 3570 | 7 | 25 | 4 |
| 3570 | 2.5 | 9 | 6 |
| 10700 | 14.5 | 155 | 1.4 |
| 10700 | 6.5 | 70 | 1.9 |
| 10700 | 4 | 43 | 2.5 |
| 10700 | 2 | 21 | 4 |
| 10700 | 1 | 11 | 6 |

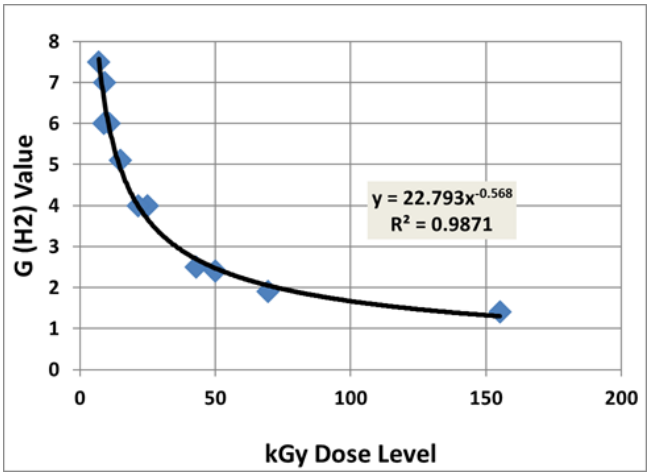


**Figure 5-7. Data points from Figure 5-6/Table 5-2 for multiple dose rates plotted as a function of dose, with a power-law fit (G in units of molecules of $H_2$ per 100 eV energy desposited)**

**Table 5-3. Primary yields (in molecules/100 eV) of products of water radiolysis under different types of radiation at room temperature [Wang, 2013]**

| Source | LET (keV/$\mu$m) | g(-$H_2O$) | g($e^-_{aq}$) | g(OH) | g(H) | g($H_2$) | g($H_2O_2$) | g($HO_2$) |
|---|---|---|---|---|---|---|---|---|
| $^{60}$Co $\gamma$-ray [39] | 0.23 | 4.08 | 2.63 | 2.72 | 0.55 | 0.45 | 0.68 | 0.008 |
| $H^+$ [39] | 12.3 | 3.46 | 1.48 | 1.78 | 0.62 | 0.68 | 0.84 | - |
| Fast neutron [40] | 40 | 3.19 | 0.93 | 1.09 | 0.50 | 0.88 | 0.99 | 0.04 |
| $He^{2+}$ [39] | 108 | 2.84 | 0.54 | 0.54 | 0.27 | 1.11 | 1.08 | 0.07 |
| $^{10}$B(N, $\alpha$)$^7$Li [41–43] | 220 | 3.9 | 0.33 | 0.30 | 0.10 | 1.8 | 1.67 | 0.13 |

## 5.2. Radiolysis in Water Films Versus Water Vapor

For the evaluation of water radiolysis in the SNF cask, two types of water are assumed to be present, water that may be present as surface adsorbed films and water vapor in the cask environment associated with humidity levels. Yousefi [Yousefi, 2014] reports results from two sources comparing $G_{H2}$ values in liquid water and water vapor. The comparison is shown in Table 5-4, first in the reported units of micromoles per joule and then converted to molecules/100 eV (1 μmol/J = 9.63 molecules/100 eV). The values were obtained from [Elliott, 2009] and [Arkhipov, 2007]. There is a significant difference in the G-value of most species for liquid versus vapor, but the $G_{H2}$ value is similar for both, with the vapor value being slightly higher. Other reported values for $G_{H2}$ for steam and water vapor vary from 0.05 [Boyd, 1973] to >2 (beta radiation at elevated temperature) [Boyd, 1963]. $G_{H2}$ for pure liquid water is reported by [Crumière, 2013] as 0.25-0.30 molecules/100 eV as compared to a typical value of 0.46 molecules/100 eV in a system where a substrate is present on which the water can be physisorbed or chemisorbed. Liquid water is assumed not to be present in the cask, so a $G_{H2}$ for liquid water will not be used. The value for water vapor based on [Arkhipov, 2007] of 0.47 molecules/100 eV will be used for the comparative calculations.

**Table 5-4. Primary yields of water radiolysis under γ irradiation 25°C [Youssefi, 2014], as originally reported in μmol/J and converted to molecules/100 eV**

| Water phase | G units | $H_2O$ | $\cdot e_{aq}^-$ | $H^+$ | ·OH | ·H | $H_2$ | O | $H_2O_2$ |
|---|---|---|---|---|---|---|---|---|---|
| Liquid [Yousefi, 2014] | μmol/J | -0.41 | 0.26 | 0.26 | 0.27 | 0.06 | 0.04 | 0.0 | 0.07 |
| Vapor [Yousefi, 2014] | μmol/J | -0.74 | 0.0 | 0.0 | 0.63 | 0.74 | 0.05 | 0.11 | 0.0 |
| Liquid | molecules/100 eV | -3.9 | 2.5 | 2.5 | 2.6 | 0.58 | 0.4 | 0.0 | 0.7 |
| Vapor | molecules/100 eV | -7.1 | 0.0 | 0.0 | 6.1 | 7.1 | 0.5 | 1.1 | 0.0 |

## 5.3. Radiolytic Hydrogen Production

Based on the water source evaluation, only the water associated with the fuel rod surface chemisorption, water vapor, and the aluminum rails are potential significant contributors of the $H_2$ radiolysis production. For water chemisorbed or physisorbed on oxides (i.e., water associated with the aluminum or fuel rod surfaces), the mass of the oxides (rather than just the water content) is used to calculate the absorbed energy for the time period. The radiolytic $H_2$ production is estimated using a dose rate of $3 \times 10^{15}$ eV/g/s [Shukla, 2019] and a time period of 12 days, corresponding to the time interval of the third gas sample taken from the cask after sealing. The total dose for the 12-day period (assuming constant dose rate) is $(3.00 \times 10^{15}\ \text{eV}/(\text{g}\cdot\text{s}))(12\ \text{days}) = 3.11 \times 10^{21}\ \text{eV/g} = 3.11 \times 10^{19}\ 100\ \text{eV/g}$.

### 5.3.1. Aluminum Components

For aluminum (oxy)hydroxide sources, the total mass of (oxy)hydroxide is calculated based on the estimated exposed aluminum surface area, the assumed (oxy)hydroxide layer thickness, and the density of the (oxy)hydroxide (2.53 g/cm$^3$ for bayerite and 3.01 g/cm$^3$ for boehmite [Wefers, 1987]). The absorbed energy (in 100 eV) is calculated by multiplying the (oxy)hydroxide mass by the total dose. To account for limited $H_2$ sources, the predicted radiolytic $H_2$ yield over 12 days is either the absorbed energy multiplied by $G_{H2}$ for the (oxy)hydroxide *or* the total $H_2$ inventory of the (oxy)hydroxide, whichever is smaller.

Assuming 8 μm of bayerite remaining as bayerite after drying, the mass of oxide is about 1750 g, containing 605 g or 33.6 mol $H_2O$. The predicted yield from bayerite over 12 days with a $G_{H2}$ of 0.02 molecules/100 eV is 0.00180 mol $H_2$, a small fraction of the total inventory in the bayerite. Dividing by the estimated 386 mol He in the cask yields 4.67 ppmv.

Alternatively, assuming 5.2 μm of boehmite (corresponding to complete drying of 8 μm bayerite), the mass of oxide is about 1340 g, containing 201 g or 11.2 mol $H_2O$. The predicted yield from boehmite over 12 days with a $G_{H2}$ of 0.05 molecules/100 eV is 0.00347 mol $H_2$, a small fraction of the total inventory in the boehmite. Dividing by the estimated 386 mol He in the cask yields 8.98 ppmv.

Note that bayerite corresponds to a larger total water inventory that could be released over the long term, but (based on currently available $G_{H2}$ data) is predicted to release it more slowly than boehmite. For either assumption, the predicted yield after 12 days is low.

Details of the cask design are not readily available, and the aluminum surfaces forming the cells and associated with the neutron absorbers are not included in the base aluminum surface calculation. Performing a similar analysis to that for the aluminum rails for the aluminum surfaces in the cell matrix (assumed not to be exposed) predicts a 12-day yield of 0.00529 mol / 13.7 ppmv $H_2$ assuming bayerite and 0.0102 mol / 26.3 ppmv $H_2$ assuming boehmite, i.e., although these surfaces could potentially hold a large inventory of chemisorbed water, the impact on the 12-day radiolytic $H_2$ would be relatively small.

### 5.3.2. Fuel Rod and Other Zr Surfaces

For the fuel rod surface water, the same type of calculation applies, except for the handling of the water inventory. The initial surface water on the $ZrO_2$ is based on three molecular layers of water on the surface (with additional effective surface area due to fissures and crud). For the assumption of replenishment, as this water is depleted by radiolysis, it can adsorb additional water from the water vapor in the gas to maintain an equilibrium balance between adsorbed and gas-phase water. A conservative estimate is that the total inventory of free and surface water be used as the limiting inventory for radiolysis from all of these inventories. As a result, the radiolytic yield will first be calculated for the Zr components, water vapor, and steel surfaces and then the sum of these yields will be the $H_2$ production from the combined free and surface water inventory.

The absorbed energy is calculated for the full oxide mass, assuming an average $ZrO_2$ thickness of 39 μm on the fuel rods (half that thickness on the other Zr components) and $ZrO_2$ density of 5.68 g/cm$^3$. This is a conservative approach, since not all of the energy absorbed by the $ZrO_2$ oxide will be directly applied to the surface radiolysis.

The estimated $ZrO_2$ mass on the fuel rods is about 257 kg (217 kg for the fuel rods with 39-μm-thick oxide and 40 kg for the additional Zr components with 19.5-μm-thick oxide). The predicted yield based on $G_{H2}$ and the 12-day absorbed dose for the $ZrO_2$ is 5.26 mol $H_2$ (equivalent to 13600 ppmv) for the fuel rods and 0.973 mol $H_2$ (equivalent to 2520 ppmv) for the additional Zr surface.

### 5.3.3. Water Vapor

An initial 2% (20000 ppmv) water vapor content is used as a preliminary estimate to calculate the impact of water vapor content on the radiolysis. This water content corresponds to an estimated 7.72 mol / 139 g water vapor (based on the estimated moles of gas in the cask). The predicted radiolytic $H_2$ generation over the 12-day period (water vapor mass multiplied by the dose and $G_{H2}$ for water vapor) is 0.0034 mol $H_2$, corresponding to 8.7 ppmv.

### 5.3.4. Steel Surfaces

For the steel surface, the radiolytic yield is calculated using the water $G_{H2}$ of 0.47 molecules/100 eV and the estimated 237 g of physisorbed/chemisorbed water initially predicted on the steel surface, which predicts $5.76\times10^{-6}$ mol $H_2$ (<1 ppmv) over 12 days.

For the case of water replenishment of the fuel surface (with $ZrO_2$), the total predicted radiolytic yield from free and surface water over 12 days is 6.24 mol $H_2$, equivalent to 16100 ppmv, which is about

78.5% of the total estimated free and surface water inventory. The total radiolytic $H_2$ is overwhelmingly dominated by that from the Zr surfaces due to the assumption of energy transfer from the oxide to the adsorbed water.

# 6. RESULTS AND DISCUSION

The water content, post-dryout, of the HBU Demonstration cask and the radiolysis of those waters causing hydrogen production, were estimated. Potential consumption of hydrogen by gettering by the fuel clad and other zirconium alloys was not estimated. Chemical back reactions were not considered.

A number of assumptions were made in estimating contributions to the free, physisorbed, and chemisorbed waters associated with the fuel rod surface and structural components in the cask, and the hydrogen generation therefrom. This study constructs a component-residual water content set and estimates the total hydrogen and the hydrogen production rate via radiolysis of this set to identify the primary $H_2$ sources and their relative impacts.

Table 6-1 shows the calculated values of both potential total inventory and 12-day and 40-year radiolytic generation levels. These values are to be considered relative and qualitative. The specific assumptions and estimates made in the calculations are contained in the body of this report. For the 40-year analysis, the dose rate was assumed to decay exponentially from the initial value with the half-life of Cs-137 (30.05 y); therefore, the $3\times10^{15}$ eV/g/s dose rate used in the calculation was multiplied by $(40\text{ y})^{-1}\int_{0\text{ y}}^{40\text{ y}}\exp\left(-\frac{\ln(2)t}{30.05\text{ y}}\right)dt = 0.653$ to account for the average dose rate over the 40-year span.

**Table 6-1 Hydrogen production due to radiolysis in the HBU Demonstration Cask**

| **$H_2$ Source** | **Total $H_2$ inventory (ppmv)** | **$H_2$ production in 12 days (ppmv)** | | | | **$H_2$ production in 40 years (ppmv)** |
|---|---|---|---|---|---|---|
| | | **Assuming no $H_2O$ replenishment of surface water (Case 1)** | | **Assuming rapid $H_2O$ replenishment of surface water from water vapor (Case 2)** | | **Assuming $H_2O$ replenishment** |
| Free/surface water | 20554 | 0.01 | (steel) | 0.01 | (steel) | 20554 |
| | | 520.3 | ($ZrO_2$) | 16133 | ($ZrO_2$) | |
| | | 8.7 | (vapor) | 8.7 | (vapor) | |
| Chemisorbed water (bayerite on rails) | 86946 | 4.67 | | 4.67 | | 3711 |
| **Total $H_2$** | **107500** | **534** | | **16146** | | **24265** |
| Chemisorbed water (bayerite on cell matrix components) | 254816 | 13.7 | | 13.7 | | 10875 |

The results from the calculations for a 12-day exposure in the HBU Demonstration cask are:

A. The calculated $H_2$ production from the aluminum rails (assuming bayerite) is 4.67 ppmv.
B. The calculated $H_2$ production from the water vapor is 8.7 ppmv
C. The calculated $H_2$ production from the fuel rod surface water is 520 ppmv (for case 1 of no replenishment of the initial ascribed water) and 16100 ppmv (for case 2 of full replenishment of the initial water). This second case significantly exceeds the amount of physisorbed/chemisorbed water estimated to initially be on the Zr component surfaces. It is assumed that exchange with the water vapor will replenish the surface water until all water vapor and exchangeable surface water is depleted. The high production quantity from the fuel rod is a result of the relatively large $ZrO_2$

mass to absorb radiation energy. The inclusion of the total oxide mass for dose accumulation is conservative.

D. Radiolysis on the steel surfaces does not contribute significant radiolytic $H_2$.

E. The inclusion of the cell matrix aluminum surfaces and the absorber surfaces do not significantly impact the short term $H_2$ but can impact the longer-term generation if included. A more detailed evaluation of the specific cell matrix design is needed to determine what surface areas are appropriate to address. The tri-hydrated oxide (bayerite) with a conservative (large) thickness of 8 μm was assumed for the water source in Table 6-1.

**Recommendations for refinements to the hydrogen generation estimation spent fuel in dry storage canisters:**

Dose rates are necessary to determine radiolytic hydrogen production. Estimates of dose rates with ranges have been reported, but specific dose rates (spatial- and temporal-dependent) for the HBU cask would improve the accuracy of the radiolysis calculations.

The results in this report show that the radiolysis occurring on the zirconium alloys with attendant $ZrO_2$ oxide and crud surface films is the major contributor of hydrogen for the short-term cask atmosphere. The fact that the predicted 12-day value for $H_2$ for case 2 (16146 ppmv) is so much greater than that measured by Bryan et al. [Bryan et al, 2019a] (~500 ppmv) suggests that the replenishment of surface waters did not occur. The high temperature of the fuel may preclude water adsorption by the $ZrO_2$ oxide. The temperature and water vapor regime to drive replenishment were not evaluated in this present work. Information on the sister rod examinations can provide data to improve some of the parameter assumptions such as oxide thickness and rod surface characteristics would help refine input on the surface characteristics, initial water content, and potential for hygroscopic behavior for water replenishment of the fuel rod surfaces.

The aluminum components represent the largest $H_2$ reservoir in the model, but are expected to release it much more slowly than the other sources. Since the radiolysis of the aluminum oxide has the greatest potential for $H_2$ production over the long term, better characterization of the likely hydrated oxide formed on the cask internals, its condition post-dryout, and the determination/verification of steady state G-values for the residual aluminum hydrated oxides is important for accurate estimation of the hydrogen build-in the cask long-term.

The fuel and internals in a spent fuel cask provide several surface conditions and potential for physisorbed/chemisorbed materials and conditions. The literature information cited in this report provided a basis for estimation of radiolytic hydrogen gas generation in a SNF canister. Additional testing and modeling of these materials under radiolysis conditions would help refine the inputs and assumptions in the estimation.

**Concept for in integrated system for radiolysis testing**: The lack of consensus test standards for material-specific radiolytic gas yields and the materials interactions in a closed system challenge the application of literature information and the overall estimation of water radiolysis in an SNF canister. An integrated test is suggested.

A “mini-canister” or small stainless steel vessel would be loaded with Zry cladding material (with appropriate surface oxide condition) and controllable heating, aluminum material (with appropriate hydrated oxide condition) with appropriate surface-to-surface ratios, and surface-to-free volume ratios matched to SNF canisters. The inventories of water associated with the materials would be quantified. The mini-canister radiolysis test would be staged in a $^{60}Co$ irradiator. The gas space would be sampled periodically on-line to provide characterization of the $H_2$ evolution. This test system and modeling thereof would provide information to improve the estimation of radiolysis in SNF canisters with residual water. This concept would be further developed in FY21 under the NE-SFWST program.

# 7. REFERENCES

Agayev, T. N., Faradj-zadeh, I. A., Aliyev, A. G., Eyubov, K. T., & Aliyev, S. M. (2017). “Regularities of radiation and heterogeneous processes in contact of Zr and Zr1% Nb alloy with water”. Вопросы атомной науки и техники.

Al-Abadleh, H.A and Grassian, V. H.; “FT-IR Study of Water Adsorption on Aluminum Oxide,” Langmuir 2003, Vol 19 pages 341 – 347.

Arkhipov, O. P., Verkhovskaya, A. O., Kabakchi, S. A., & Ermakov, A. N. (2007). Development and verification of a mathematical model of the radiolysis of water vapor. Atomic energy, 103(5), 870-874.

ASTM International. “Standard Guide for Drying Behavior of Spent Nuclear Fuel.” ASTM C1553–16. West Conshohocken, Pennsylvania: ASTM International. 2016.

Boyd, A. W., and O. A. Miller. "Radiolysis of water vapor with fission fragments." Canadian Journal of Chemistry 46.24 (1968): 3773-3778.

Boyd, A. W., C. Willis, and O. A. Miller. "The Radiolysis of Water Vapor at Very High Dose Rates. I. Hydrogen Yields from H2O, H2O–HCl, and H2O–HBr Mixtures." Canadian Journal of Chemistry 51.24 (1973): 4048-4055.

Bryan, Charles, Russell Jarek, Chris Flores, Elliott Leonard: High Burn-up Demonstration Cask: SNL Gas Analyses: Sandia National Laboratories ASTM Nuclear Fuel Drying Workshop January 29, 2019a; also in SNL report Bryan, Charles R., Russell L. Jarek, Chris Flores, Elliott Leonard, Analysis of Gas Samples Taken from the High Burnup Demonstration Cask, Sandia National Laboratories, SANDIA REPORT SAND2019-2281.

Bryan, C.R., S.G. Durbin, E. Lindgren, A.G. Ilgen, T.J. Montoya, T. Dewers, D. Fascitelli. “SNL Contribution: Consequence Analysis for Moisture Remaining in Dry Storage Canisters After Drying,” Sandia National Laboratory, SAND2019-8532 R, 2019b.

Byers, W.A.; "Pressurized water reactor core crud mapping," in 18th international conference on nuclear engineering (ICONE 18), Xian China, 2010.

CNWRA. Extended Storage and Transportation: Evaluation of Drying Adequacy. Authors: H. Jung, P. Shukla, T. Ahn, L. Tipton, K. Das, X. He, and D. Basu, San Antonio, Texas: Center for Nuclear Waste Regulatory Analyses. 2013.

Crumière, F., Vandenborre, J., Essehli, R., Blain, G., Barbet, J., & Fattahi, M. (2013). LET effects on the hydrogen production induced by the radiolysis of pure water. Radiation Physics and Chemistry, 82, 74-79.

d’Entremont, A. L., Fuentes, R. E., Shalloo, M. G., Knight, T. W., Sindelar, R. L., Thermal Dehydration of Aluminum (Oxy)hydroxides on Fuel Cladding Material, Proceedings of Waste Management Symposia 2020, #20200, 2020.

Dylla, H.F.; "The Problem of Water in Vacuum Systems", presentation at CERN Accelerator School May 2006

Elliot, A. J., and D. M. Bartels." The reaction set, rate constants and g-values for the simulation of the radiolysis of light water over the range 20° to 350°C based on information available in 2008". No. AECL—153-127160-450-001. Atomic Energy of Canada Limited, 2009.

Elliot, A.J., . Bartel, D. M., AECL Report-11073, Chalk River, Canada, 2009

Fort, James A., D.J. Richmond, J.M. Cuta, S.R. Suffield, “Thermal Modeling of the TN-32B Cask for the High Burnup Spent Fuel Data Project”, July 30, 2019,PNNL-28915

Hazelton, R.F.;"Characteristics of Fuel Crud and its Impact on Storage, Handling, and Shipment of Spent Fuel" - September 1987 Prepared for the U.S. Department of Energy under Contract DE-AC06-76RLO 1830 Pacific Northwest Laboratory Richland, Washington 99352 PNL--6273 DE88 000914

Garibov, A.A., T.N. Agayev, G.T. Imanova, K.T. Eyubov, “Kinetics of radiation and catalytic decomposition of water in the presence of nano-zirconium dioxide.” issn 1562-6016. PAST. 2015. №5(99), p. 48.

Hering, G. ;"Spent Nuclear Fuel Storage Demo Heats Up: Ten-Year Demonstration to Begin in 2017", EPRI Journal, 2016, 26–28.

Holmes, H. F., Fuller Jr, E. L., & Beh, R. A. (1974). “Adsorption of argon, nitrogen, and water vapor on zirconium oxide”. Journal of Colloid and Interface Science, 47(2), 365-371.

Horne, G.P., S.M. Pimblott, J.A. LaVerne, “Inhibition of Radiolytic Molecular Hydrogen Formation by Quenching of Excited State Water”. Journal of Physical Chemistry B 121, 2017, 5385-5390.

Hou, B., Kim, S., Kim, T., Kim, J., Hong, S., Bahn, C. B., ... & Kim, J. H. “The hydration structure at yttria-stabilized cubic zirconia (110)-water interface with sub-Ångström resolution”. *Scientific reports*, *6*, 27916. (2016).

Jenson, B. ;“TN 32 Dimensions For Thermal Analysis”, Drawing of TN-32 cask provided courtesy of K. Waldrop, EPRI.

Kabakchi, S.A.,O.P. Arkhipov, M.L. Lukashenko: " Specific Features of the Radiolysis of Water and Aqueous Solutions of H2 and O2 by Mixed n,γ-Radiation with a High Portion of the Neutron Component.", High Energy Chemistry 47, 2013, 147-151.

Kaddissy, J.; "Hydrogen production from irradiated aluminum hydroxide and oxyhydroxide". PhD thesis. Material chemistry. Université Paris-Saclay, 2016.

Knoll, R.W., et al., “Evaluation of Cover Gas Impurities and Their Effects on the Dry Storage of LWR Spent Fuel,” PNL-6365, DE88 003983, PNNL, November 1987.

Knott, R. P., Kesterson, R. L., Hallstadius, L. G., & Young, M. Y. (2003, March). “Advanced PWR fuel designs for high duty operation”. In Proceedings from the ENS TopFuel 2003 Meeting (pp. 16-19).

Köck, E. M., Kogler, M., Klötzer, B., Noisternig, M. F., & Penner, S. (2016).” Structural and electrochemical properties of physisorbed and chemisorbed water layers on the ceramic oxides Y2O3, YSZ, and ZrO2”. ACS applied materials & interfaces, 8(25), 16428-16443

LaVerne, J.A.,L. Tandon,; "H2 Production in the Radiolysis of Water on UO2 and Other Oxides". J. Phys. Chem. B 107, 2003, 13623-13628.

Le Caër, S.; " Water Radiolysis: Influence of Oxide Surfaces on H2 Production under Ionizing Radiation", Water 3, 2011, 235-253.

Montgomery, R., John M. Scaglione, Bruce Bevard, “Post-irradiation Examinations of High Burnup PWR Rods” –18456 WM2018 Conference, March 18–22, 2018, Phoenix, Arizona, USA

Pastina. B. and LaVerne,J. A. "Effect of Molecular Hydrogen on Hydrogen Peroxide in Water Radiolysis", J. Phys. Chem. A 2001, 105, 9316-9322.

Petrik, N. G., Alexandrov, A. B., & Vall, A. I. (2001).” Interfacial energy transfer during gamma radiolysis of water on the surface of ZrO2 and some other oxides”. The Journal of Physical Chemistry B, 105(25), 5935-5944.

Poloski, A., Hanson, B. " Initial Concepts for a Small Scale Drying Study" ASTM Subcommittee C26.13 Meeting – Spent Fuel and High Level Waste January 28, 2019

Shukla, P, R.L. Sindelar, P.-S. Lam, “Consequence Analysis of Residual Water in a Storage Canister – Preliminary Report,” SRNL−STI−2019−00495

Sindelar, R.L., M.J. Connolly, J.J. Jarrell, D.T. Herman, and W.H. Bates, *Technology Development for Dry Storage of Aluminum-Clad Spent Nuclear Fuel*, Paper 20490 at WM2020, March 2020.

Skotnicki, K., & Bobrowski, K.; “Molecular hydrogen formation during water radiolysis in the presence of zirconium dioxide.” Journal of Radioanalytical and Nuclear Chemistry, 304(2), 473-480. (2015)

Spinks,J. W., Woods, R.J.; "An Introduction to Radiation Chemistry", 3rd ed., Wiley Interscience, New York, 1990.

Waldrop,K. “RE: [EXTERNAL] cask design.” Received by Robert Sindelar, 08 July, 2020.

Wang, M.; " Irradiated Assisted Corrosion of Stainless Steel in Light Water Reactors" – Focus on Radiolysis and Corrosion Damage. hal-00841142, 2013

Wefers,K. and Misra,C.; "Oxides and hydroxides of aluminum," Alcoa Laboratories Pittsburgh, PA Alcoa Technical Paper #19, 1987.

Wertsching, A. K. "Material Interactions on Canister Integrity during Storage and Transport." DOE/SNF/REP-104 (2007)

Westbrook,M.L. R.L. Sindelar, D.L. Fisher, "Radiolytic hydrogen generation from aluminum oxyhydroxide solids: theory and experiment." J. Radioanalytic and Nuclear. Chem. 303, 2015, 81-86.

Wittman, R.S.; "Radiolysis Model Sensitivity Analysis for a Used Fuel Storage Canister", FCRD-UFD-2013-000357, PNNL-22773, 2013.

Wilson, W., and R. J. Comstock. Potential impacts of crud deposits on fuel rod behavior on high powered PWR fuel rods. No. IAEA-TECDOC--1128. 1999.

Yousefi, N. "Gamma-Radiolysis Kinetics of Liquid, Vapour and Supercritical Water.", Master’s thesis, University of Western Ontario, 2014.